Trends in Electron-Deficient Bridges

Georges Trinquier* and Jean-Paul Malrieu

Contribution from the Laboratoire de Physique Quantique, C.N.R.S., U.R.A. No. 505, Université Paul-Sabatier, 31062 Toulouse Cedex, France. *Received May 3, 1991*

Abstract: A previously defined procedure, based on orthogonal valence bond decomposition of a correlated wave function, is applied to nine doubly bridged electron-deficient systems isoelectronic with diborane: X_2H_6 (X = B, Ga), X_2H_4 (X = C, Si, Ge, Sn, Pb), and $X_2H_6^{2+}$ (X = C, Si). Basic features are found to be common to all species, such as the high separability of the bridges and the primacy of X–H–X peripheral bonding over X–X central bonding. Other electronic properties exhibit regular and consistent variations. The electron population on the bridging hydrogens H_b summarizes these trends and may be used to set up a continuous scale. Simple modeling of a single bridge suggests that its changes can arise from two factors: orbital electronegativity differences, and the architecture of the interactions, ranging between two limiting forms (schematized by the cyclopropenyl cation, with all centers bound, and the allyl cation, with only 1–2 and 2–3 binding). Direct evaluation of the transfer integrals shows that the second factor is not the leading one since the through-space/through-bond ratios are rather constant along the series, except for $C_2H_6^{2+}$ which undergoes more through-space C–C binding. The distribution of the compounds along the scale is therefore mainly governed by electronegativity factors. The ordering ($C_2H_6^{2+}$, C_2H_4, B_2H_6, $Si_2H_6^{2+}$, Si_2H_4, Ga_2H_6, Ge_2H_4, Sn_2H_4, Pb_2H_4) indicates, among other things, an increase in electron population on H_b and a decrease in interbridge delocalization (which remains weak in any case). The various components of the energies of fragment dimerization into double bridges are calculated and discussed. Possible views for the diprotonation of X_2H_4 are provided. Structures of peculiar singly bridged systems are also examined.

I. Introduction

Three-center two-electron double bridges exist not only in diborane (B_2H_6) and its heavier analogues but also in various isoelectronic species. The ethane dication ($C_2H_6^{2+}$) exhibits a D_{2h} symmetrical doubly bridged structure, **1**, as a local minimum lying about 9 kcal/mol above the preferred C_{2v} arrangement.[1,2] While

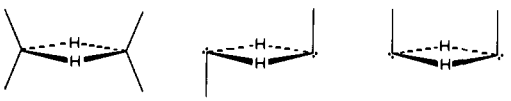

1 **2** **3**

doubly bridged forms are not local minima on the potential energy surface of C_2H_4, these happen to be true minima for all its heavier analogues in group 14.[3] The C_{2h} trans form, **2**, slightly favored with respect to the C_{2v} cis form, **3**, is the absolute minimum for Sn_2H_4 and Pb_2H_4.

In a preceding paper, we applied a general method of analysis of electronic structures to the double bridge of diborane.[4] This procedure is based on an OVB expansion of the correlated wave function associated with a given chemical group. The method proved to be efficient in showing the degree of independence of the bridges and the relative extent of direct bonding along B–H and B–B. The study concluded that there was a significant prevalence of the B–H binding interactions over the direct B–B ones, which however are not negligible.

The relative importance of XH vs XX interactions has no reason to be constant when going from one system to an isoelectronic one involving different X atoms or different surroundings or net charges. The preceding analysis concluded that each B–H–B bridge in B_2H_6 stands approximately halfway between the two limiting forms of the two-electron three-center bond, namely the H_3^+-like or cyclopropenyl cation like system and the allyl cation like system. It may be tempting to see whether, in a large series of electron-deficient double bridges, the XH/XX interaction ratio significantly varies and whether these two asymptotic forms can be approached. Our analysis of the diborane molecule used well-defined general procedures and original indexes (such as the CORP index) which can be applied to other compounds as well.

We would like, in the present work, to apply these tools to the analysis of the three types of above-mentioned electron-deficient double bridges. The following examples were chosen for our comparative study: (1) B_2H_6 and one of its heavier analogues, the recently prepared[5] and theoretically studied[6,7] digallane (Ga_2H_6); (2) $C_2H_6^{2+}$ in its D_{2h} form, which can be seen as the dication of ethane or the diprotonated form of ethylene, and one of its heavier analogues $Si_2H_6^{2+}$, which has not been detected or theoretically explored to date; and (3) the series of trans doubly bridged X_2H_4 for all of group 14, recently studied.[3] Note that C_{2h} C_2H_4 is included in the series for the sake of completeness, although this form is not a real minimum on the potential energy surface and is located very high in energy (>150 kcal/mol) above the stable D_{2h} ethylene. This results in a series of nine compounds, one of them not being a true minimum.

After a brief recap of the method (Section II), we shall class the observed electronic trends (Section III) and try to understand and rationalize them (Section IV). Next, two specific points will be addressed: dimerization energies (Section V) and extension to peculiar single bridges (Section VI).

II. Procedure and Tools

The geometries for all systems are optimized at the SCF-DZP level. For group 14 X_2H_4, these have been given in ref 3. The remaining geometries are given in Section I of the Appendix, together with the corresponding vibrational frequencies and all of the theoretical details regarding basis sets and programs. Let us recall briefly the procedure we used to analyze the bonding in our selected double bridges. It consists of four steps: (1) A CASSCF multiconfigurational Hartree–Fock calculation is performed over the active space defined by the six orbitals and four electrons of the double-bridge region. This best describes the valence (or nondynamical) correlation for the ring electrons, as confirmed by the nature of the six concerned orbitals which remain concentrated on the X_2H_2 ring. (2) The active-space orbitals are then localized into a set of NAMOs (*nearly atomic molecular orbitals*), i.e. a minimal set of orthogonal molecularly adapted atomic orbitals. (3) Next, these orbitals are used to build a basis set of orthogonal valence bond (OVB) determinants on which the

(1) Olah, G. A.; Simonetta, M. *J. Am. Chem. Soc.* **1982**, *104*, 330.
(2) Schleyer, P. v. R.; Kos, A. J.; Pople, J. A.; Balaban, A. T. *J. Am. Chem. Soc.* **1982**, *104*, 3771.
(3) Trinquier, G. *J. Am. Chem. Soc.* **1990**, *112*, 2130.
(4) Trinquier, G.; Malrieu, J. P.; Garcia-Cuesta, I. *J. Am. Chem. Soc.* **1991**, *113*, 6465.
(5) Downs, A. J.; Goode, M. J.; Pulham, C. R. *J. Am. Chem. Soc.* **1989**, *111*, 1936. Pulham, C. R.; Downs, A. J.; Goode, M. J.; Rankin, W. H.; Robertson, H. E. *J. Am. Chem. Soc.* **1991**, *113*, 5149.
(6) Liang, C.; Davy, R. D.; Schaefer, H. F., III *Chem. Phys. Lett.* **1989**, *159*, 393.
(7) (a) Lammerstsma, K.; Leszczynski, J. *J. Phys. Chem.* **1990**, *94*, 2806. (b) Lammerstsma, K.; Leszczynski, J. *J. Phys. Chem.* **1990**, *94*, 5543.

0002-7863/91/1513-8634$02.50/0

Table I. OVB Weights (%) of the Space Part Configurations

	B_2H_6	Ga_2H_6	$C_2H_6^{2+}$	$Si_2H_6^{2+}$	C_2H_4	Si_2H_4	Ge_2H_4	Sn_2H_4	Pb_2H_4
Φ_1	7.87	8.45	6.42	8.01	7.12	8.46	9.04	9.17	9.94
Φ_2	6.49	7.58	4.72	6.88	4.88	7.16	7.52	7.99	4.17
Φ_3	4.92	4.81	6.05	5.03	5.47	4.97	4.75	4.59	4.10
Φ_4	3.61	4.14	1.47	3.84	2.17	4.09	4.43	4.62	5.35
Φ_5	3.27	2.86	6.06	3.33	4.90	3.19	2.76	2.48	1.87
Φ_6	2.65	2.52	1.99	2.71	2.24	2.60	2.51	2.44	2.36
Φ_7	1.62	2.11	0.29	1.88	0.70	2.18	2.45	2.58	3.25
Φ_8	1.60	1.44	2.29	1.46	2.11	1.56	1.49	1.45	1.28
Φ_9	1.06	1.14	1.25	1.06	0.98	1.09	1.00	1.07	0.88
Φ_{10}	0.84	0.75	1.64	0.81	1.24	0.83	0.71	0.67	0.48
Φ_{11}	0.81	0.50	1.17	0.69	1.24	0.39	0.33	0.25	0.21
Φ_{12}	0.73	0.68	0.58	0.69	0.60	0.68	0.65	0.66	0.61
Φ_{13}	0.44	0.25	0.30	0.34	0.45	0.20	0.18	0.13	0.12
Φ_{14}	0.37	0.21	0.69	0.30	0.77	0.19	0.15	0.11	0.08
Φ_{15}	0.34	0.25	0.81	0.27	0.71	0.32	0.28	0.25	0.19
Φ_{16}	0.32	0.20	0.42	0.26	0.41	0.15	0.13	0.11	0.09
Φ_{17}	0.21	0.11	0.25	0.16	0.35	0.10	0.08	0.06	0.05
Φ_{18}	0.20	0.10	0.21	0.15	0.25	0.09	0.08	0.06	0.04
Φ_{19}	0.16	0.09	0.31	0.13	0.34	0.08	0.07	0.05	0.04
Φ_{20}	0.14	0.15	0.23	0.14	0.14	0.15	0.12	0.13	0.08
Φ_{21}	0.13	0.08	0.22	0.11	0.21	0.07	0.06	0.04	0.03
Φ_{22}	0.01	0.00	0.02	0.01	0.04	0.00	0.00	0.00	0.00
Φ_{23}	0.01	0.00	0.02	0.00	0.02	0.00	0.00	0.00	0.00
Φ_{24}	0.01	0.00	0.01	0.01	0.00	0.00	0.00	0.00	0.00
Φ_{25}	0.01	0.00	0.01	0.00	0.01	0.00	0.00	0.00	0.00
Φ_{26}	0.00	0.00	0.00	0.00	0.00	0.00	0.00	0.00	0.00
Φ_{27}	0.00	0.00	0.00	0.00	0.00	0.00	0.00	0.00	0.00
Φ_{28}	0.00	0.00	0.00	0.00	0.00	0.00	0.00	0.00	0.00
S^a	4.58	4.44	4.70	4.52	4.73	4.43	4.37	4.33	4.23

[a] Entropies calculated over the 225 determinant distributions.

initial wave function is reexpressed, providing both a picture of the electron distribution and a hierarchy of local situations. (4) The resulting OVB weights are lastly processed in order to trace the physical effects and to assign electronic populations and their fluctuations to each NAMO and given subsets of NAMOs.

In step 2, Boys' localizing procedure leads to two NAMOs centered on the bridging hydrogens, h and h', and four equivalent hybrids directed along the B–H or X–H bonds, b_1, b_2, b'_1, and b'_2, **4**. The distribution expressed in this basis will be used for

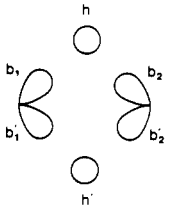

4

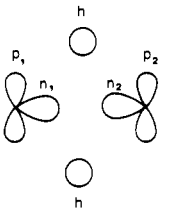

5

most of the discussion, but there is also an equivalent set obtained by further combining the b and b' hybrids into n and p orbitals and keeping the h NAMOs unchanged, **5**. This distribution will be used in some instances and one may note that it is particularly relevant for X–X bound systems since the n_1 and n_2 NAMOs point toward each other along the XX axis.

The results are summarized through the following values. The raw information first comes from the complete distribution of the CASSCF wave functions over the b and h NAMOs. It is further reduced to the following: (1) The first index is $P^{(2)}$, the probability of finding two electrons (and only two) in a given set of orbitals, generally an orbital pair. This term is related both to the mean electron population in the orbital set and to its fluctuation. (2) The next index is the CORP index, i.e., the *covalent organization residual probability* of finding two electrons in a given pair (or subset) of NAMOs. This index measures the occurrence of two electrons in a given set which is not statistical but comes from the binding interaction. It reflects the extent of delocalization between two orbitals or two atoms. (3) The final index is the mean electron population on each NAMO and most interestingly on the hydrogen orbitals, therefore on the bridging hydrogen atoms. The two preceding points must be compared with the corresponding random distributions which would respect these charges, giving what we call weighted random values.[4] For more complete definitions of these indexes and analyses of their properties and significance, the reader is referred to ref 4.

III. Scaling the Electronic Properties

Let us examine, first, the crude OVB decomposition. The 28 space parts of the 225 determinants of the OVB decompositions for our nine systems are listed in Table I. Each configuration is given in Figure 1. The weights take into account spin degeneracies but not space degeneracies. Before reducing the information hidden in such distributions, let us make some brief comments on these numbers. The decreasing ordering of the weights for B_2H_6 (first column) is kept for the other systems except $X_2H_6^{2+}$ and C_2H_4. The concentration of the strong contributions in the first nine configurations, which keep 2 electrons in each bridge, is also maintained in all the compounds studied except $C_2H_6^{2+}$ and C_2H_4. Of the three typical neutral and ionic situations Φ_1, Φ_5, and Φ_7 (**6**), the neutral configuration Φ_1 is in all cases the

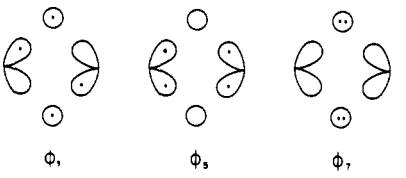

6

leading one and it has an increasing weight for heavier elements. In spite of electronegativity differences, the weight of Φ_7 is never predominant. The weight of Φ_5, on the other hand, is the second most important for $C_2H_6^{2+}$. An inversion in the Φ_5/Φ_7 ordering takes place between Ge_2H_4 and Sn_2H_4. Even for Pb_2H_4, the Φ_7 ionic contribution is still only 1/3 of that of neutral Φ_1. For Ga_2H_6, this reduces to 1/4 which does not support the basically ionic structure suggested from topological electron density analysis.[7] From B_2H_6 to Ga_2H_6, there is, as expected, a difference in the extent of ionic character, but all compounds are basically neutral in the VB sense. A measure of the dispersion of the probability

Table II. Electron Population in Each NAMO and Selected Bielectronic Probabilities[a]

		$C_2H_6^{2+}$	C_2H_4	B_2H_6	$Si_2H_6^{2+}$	Si_2H_4	Ga_2H_6	Ge_2H_4	Sn_2H_4	Pb_2H_4
	q_b	0.663	0.627	0.572	0.567	0.563	0.557	0.549	0.542	0.515
	q_h	0.674	0.745	0.856	0.866	0.874	0.886	0.902	0.915	0.970
$P^{(2)}_{b_1,h,b_2}$	CASSCF	87.9	86.1	90.9	92.8	95.6	94.7	96.3	97.2	97.8
	WR	44.0	44.1	44.7	44.7	44.8	44.9	45.1	45.2	45.8
$P^{(2)}_{b_1,b'_1,h}$	CASSCF	47.0	48.2	47.0	47.1	47.5	46.9	48.1	47.7	49.1
$P^{(2)}_{b_1,h}$	CASSCF	38.9	40.9	45.6	46.3	47.5	47.6	48.6	49.4	51.5
	WR	33.9	35.1	37.2	37.4	37.5	37.8	38.1	38.4	39.7
$P^{(2)}_{b_1,b_2}$	CASSCF	41.5	36.9	29.7	28.8	28.0	27.0	25.9	24.8	21.1
	WR	33.5	31.2	27.5	27.1	26.9	26.4	25.9	25.4	23.5
$P^{(2)}_{n_1,n_2}$	CASSCF	68.2	63.8	49.8	47.0	42.2	42.6	39.1	36.5	31.8
	WR	42.7	41.6	37.4	36.2	33.9	34.3	32.5	31.2	28.8

[a] q in electron, $P^{(2)}$ in percent. See **4** and **5** for orbital labeling. Weighted random values (WR) are given for comparison. The first two $P^{(2)}$ lines have the same WR values.

Table III. Calculated CORP Indexes[a]

NAMO subset		$C_2H_6^{2+}$	C_2H_4	B_2H_6	$Si_2H_6^{2+}$	Si_2H_4	Ga_2H_6	Ge_2H_4	Sn_2H_4	Pb_2H_4
b_1–h	CASSCF	6.2	7.6	10.8	11.1	12.2	12.1	12.7	13.3	14.4
	WR	4.2	4.5	5.2	5.2	5.3	5.3	5.4	5.5	5.9
b_1–b_2	CASSCF	9.4	6.8	2.9	2.2	1.6	1.1	0.3	−0.3	−2.2
	WR	4.1	3.4	2.5	2.4	2.3	2.1	2.1	2.0	1.6
b_1–b'_2	CASSCF	−0.2	−0.1	0.2	0.2	0.1	0.2	0.2	0.2	0.3
b_1–h′	CASSCF	0.1	0.4	0.3	0.2	0.2	0.2	0.3	0.2	0.2
h–h′	CASSCF	1.6	1.7	1.4	1.0	0.3	0.5	0.2	0.1	−0.0
	WR	4.3	5.6	7.3	7.4	7.5	7.6	7.8	7.9	8.1
n_1–n_2	CASSCF	28.8	25.7	16.0	14.0	11.1	11.3	9.0	7.6	4.8
	WR	7.2	6.9	5.5	5.1	4.4	4.5	4.0	3.6	2.9
b_1–h–b_2	CASSCF	51.8	50.1	54.5	56.1	58.9	57.8	59.2	60.0	59.8
	WR	11.1	11.1	11.3	11.4	11.4	11.4	11.5	11.5	11.8

[a] In percent. See **4** and **5** for orbital labeling. Weighted random values (WR) are given for comparison. For b_1–b_2' and b_1–h′, these are the same as for b_1–b_2 and b_1–h, respectively.

distributions within the complete sets of 225 determinants is given by the corresponding entropies S, calculated as

$$S = -\sum_{i=1}^{225} p_i \ln p_i$$

These values are given at the bottom of Table I. They display significant variations. Note in particular that the largest value of S (C_2H_4) is almost halfway between the smallest S (Pb_2H_4) and a fully disordered distribution for which $S = \ln 225 = 5.42$. Let us now go a step further in our analysis by reducing all this information.

The probabilities for having two electrons in subsets of NAMOs are given in Table II, together with the electron population in each NAMO. The CORP indexes for certain couples of NAMOs are given in Table III. In our previous study,[4] we explained the meaning of such observables. As reported, they take on more significance when compared to what is expected from the simplest distribution which would ensure the CASSCF-calculated population in each NAMO. The $P^{(2)}$ and CORP terms obtained from such weighted random distributions are also given in Tables II and III for comparison (these are referred to as WR, as opposed to CASSCF). In these tables, the ordering of our nine compounds already anticipates trends that become apparent below.

Let us first compare two species that are isoelectronic *stricto sensu*. These are B_2H_6 and $C_2H_6^{2+}$. Their geometries present a certain contrast since the angle on H_b is more acute in $C_2H_6^{2+}$ (75°) than in B_2H_6 (85°). From B_2H_6 to $C_2H_6^{2+}$, the separation of the bridges is slightly decreased since $P^{(2)}_{b_1,h,b_2}$ drops from 91% to 88%. This is further supported by the interbridge contributions to the valence correlation energies. In Table IV, the valence correlation energies for all four-electron double bridges are decomposed into the intrapair and interpair contributions, i.e. intrabridge and interbridge contributions (this decomposition was obtained by selective excitations from the MCSCF wave function). The interbridge contribution is much larger in $C_2H_6^{2+}$ than in B_2H_6 (10 vs 4 kcal/mol) whereas the intrabridge contributions are rather constant for all the compounds studied (12–14 kcal/mol). Both $P^{(2)}_{i,j}$ and the CORP indexes in $C_2H_6^{2+}$ are larger for the b–b pair than for the b–h pair. This is further confirmed when comparing these values with the weighted random expectations. In the n,p,h space partition, **5**, the n_1–n_2 interaction seems very strong, with the largest $P^{(2)}_{n_1,n_2}$ value and a very high CORP index. Note that $P^{(2)}_{b_1,h,b_2}$ is still higher than $P^{(2)}_{n_1,n_2}$ (88% vs 68%) which means that even for $C_2H_6^{2+}$ the separation between the two bridges is still the best 2/2 partitioning of the four electrons. Finally, the electron population on the bridging hydrogen q_h also drops from 0.86 to 0.67. Taking this parameter as a key index, all the trends may be tentatively interpreted as being ruled by the relative strengths of the b–h and b–b interactions. Forgetting the atomic electronegativity factors for a while, the q_h charge is related to the closeness to one of the limiting forms **7** and **8**. In the simplest

Table IV. Valence Correlation Energies (kcal/mol)

	total	intrabridge	interbridge
$C_2H_6^{2+}$	39.1	14.5	10.0
C_2H_4	37.6	13.6	10.5
B_2B_6	29.8	12.9	4.1
$Si_2H_6^{2+}$	29.1	13.3	2.5
Si_2H_4	27.2	12.5	2.2
Ga_2H_6	26.1	12.4	1.3
Ge_2H_4	27.2	12.6	2.0
Sn_2H_4	26.1	12.4	1.3
Pb_2H_4	27.2	13.0	1.2

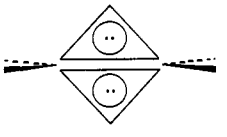

7

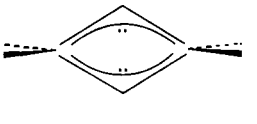

8

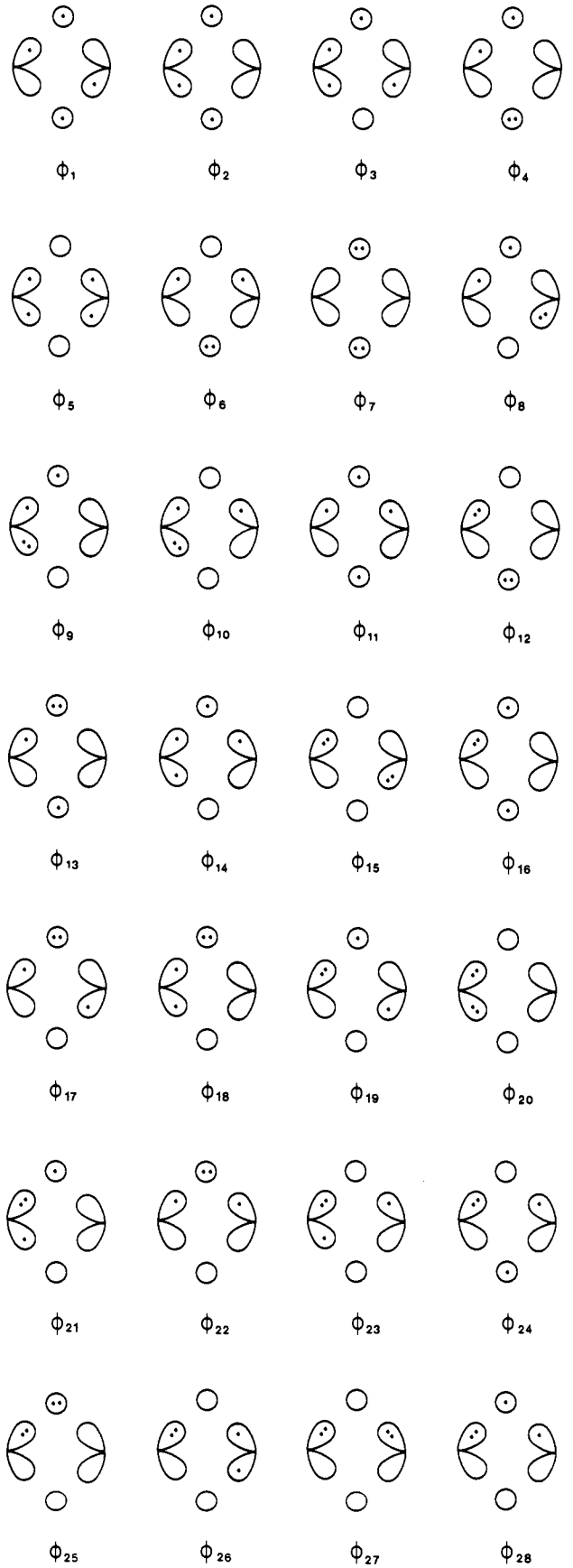

Figure 1. The 28 space parts of the orthogonal valence bond basis of determinants.

topological Hückel treatment, all orbitals would have a population of 2/3 (0.67) in **7** (imagine H_3^+ or $C_3H_3^+$) and q_h would be 1 in **8** (imagine the allyl cation). It is clear that within this assumption ignoring the atom electronegativities and according to all criteria, including the geometry, $C_2H_6^{2+}$ is very close to **7**. Thus this species would occur at one extremity of such a scale.

If we now compare B_2H_6 to Pb_2H_4, we observe that the above-discussed trends now run in the opposite direction. First, the angle on the bridging hydrogen is obtuse in Pb_2H_4 (106°). The separation of the bridges is even more pronounced in Pb_2H_4 than in B_2H_6 since $P^{(2)}_{(b_1,h,b_2)}$ increases from 91% to 98%. Pb_2H_4 thus appears as the species in which the two bridges are the most independent. This is paralleled by its small interbridge correlation energy (1 kcal/mol, see Table IV). Our indicators now suggest strong Pb–H interactions, to the detriment of direct Pb–Pb interaction. $P^{(2)}_{b_1,h}$ is increased from 46% to 52% while $P^{(2)}_{b_1,b_2}$ drops from 30% to 21%. Note that the $P^{(2)}$ term which would compete with $P^{(2)}_{b_1,h,b_2}$ is no longer $P^{(2)}_{n_1,n_2}$ (32%) but $P^{(2)}_{b_1,h}$ (52%). The CORP index for Pb–H has the largest value in the series (14%) while the CORP index for Pb–Pb is found to be negative (−2%). Again, the mean electron populations in h and b may be taken as a summary of these results. In Pb_2H_4, they are calculated at 0.51 for b_1 and b_2 and 0.97 for h. Again ignoring the possible impact of atomic electronegativity, all these results would suggest that Pb_2H_4 is very close to the limiting form **8** in which the bridges are two allylic cation like species facing each other, no longer exhibiting any link between atoms 1 and 3. Simple topological Hückel reasoning indicates that the two electrons of the allylic cation are distributed over the 1–2–3 centers as $^1/_2,1,^1/_2$ which happens to be quite close to the distribution found in the b_1,h,b_2 set for each bridge of Pb_2H_4.

The electron-deficient double bridges may therefore be ordered along a scale running between two limiting forms associated with $C_2H_6^{2+}$ and Pb_2H_4. Notably, all the compounds of our series range within this interval, as can be seen from Table II. In this table and in the following ones, the electron population in the h NAMO—which is the electron population on the bridging hydrogen H_b—has been chosen as the simplest indicator to order the various compounds. Most of the calculated observables vary monotonically along this coordinate.[8] Note that C_2H_4 is normally situated on the scale (except for $P^{(2)}_{b_1,h,b_2}$ and CORP(b_1–h–b_2)) although this structure is not a true minimum. Also, note that the terms $P^{(2)}_{b_1,b'_1,h}$ in Table II happen to be quite close to their weighted random expectations, which means that the XH_3 (or XH_2) fragments no longer exist in the doubly bridged dimers. It is not astonishing therefore that these $P^{(2)}$ terms fluctuate weakly and randomly around these weighted random values. Note, lastly, that the charge ordering happens to roughly follow the entropies of Table I, with the exceptions of C^{2+}/C and Si/Ga. Let us now comment on the trends within the families in our series.

In the three families of compounds, a "vertical" regular trend is observed going down to heavier atoms. First, from B_2H_6 to Ga_2H_6, from $C_2H_6^{2+}$ to $Si_2H_6^{2+}$, and down along the X_2H_4 series from silicon to lead there is an increase in the separation of the bridges, as indicated by $P^{(2)}_{b_1,h,b_2}$ and CORP(b_1–h–b_2) as well as by the interbridge correlation energies (see Table IV). Second, there is an increase of the X–H populations and a decrease of the X–X ones, as indicated by the $P^{(2)}$ and CORP terms for the (b,h), (b_1,b_2), and (n_1,n_2) sets. In other words, with heavier atoms, the system moves toward the right-hand side of our scale from $C_2H_6^{2+}$ (left) to Pb_2H_4 (right), according to the q_h criterion. Note that this is *partly* paralleled by the electronegativities of the atoms—we shall come back to this point in the next section.

Besides the $B_2H_6/C_2H_6^{2+}$ comparison discussed above, other "horizontal" comparisons are possible. For instance the diprotonation of X_2H_4 into $X_2H_6^{2+}$ also induces a leftward displacement along our scale, as will be seen later. On the other hand, from Ga_2H_6 to Ge_2H_4, progression is toward the right of the scale (see Tables II and III).

(8) To the exception of the pair Si_2H_4/Ga_2H_6 whose ordering would be reversed according to all observables except q_h, $P^{(2)}_{b,h}$, $P^{(2)}_{b_1,b_2}$, and CORP(b_1–b_2). Anyway these two compounds appear to have very close electron properties regarding the double bridge and can be considered to occupy about the same position in our scale.

Our selected compounds are only a few examples of electron-deficient bridges. There is little doubt that most mixed structures such as **9** with A, B = XR_2 (group 13), XR_2^+ (group 14), or XR

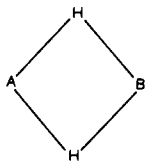

9

(group 14) are true minima on their potential surfaces, with some of them even being the absolute minimum.[9,10] The double bridges of these 135 possible combinations are expected to occupy the entire scale between our two limiting forms, thus defining an almost continuous range of formal q_n charges and associated electronic indicators.[11] As anticipated elsehwere,[4] B_2H_6 stands approximately in the middle of the interval.

IV. What Is Behind the Scale?

A. Structural and Atomic Factors. The above-mentioned consistency of the various electronic properties, calculated in the NAMO basis, along the proposed hierarchy between $C_2H_6^{2+}$ and Pb_2H_4 is striking. What may be the driving force or the leading factor under this scale?

One may first invoke structural factors. The first one might be the X–X interatomic distance in the double bridges, as compared with typical X–X single-bond lengths. The corresponding relative lengthenings[12] are plotted in function of q_h in Figure 2a. Taken as a measure of the proximity to a direct X–X single bond, the ratio $(d(\text{bridge}) - d(\text{single}))/d(\text{single})$ does not correlate with the proposed scale. Another structural observable might be the XH_bX angle, reported in Figure 2b. The correlation is now much better since this angle systematically reduces from $C_2H_6^{2+}$ to Pb_2H_4 (with the single exception of Ga_2H_6).

Since the properties of such rings may be interpreted in terms of electrostatics, one may wonder whether the leading factor is not the electronegativity differences between X and H, which could explain the variation of the net charge on the bridging hydrogen q_h. Figure 2c reports the evolution of the electronegativities (in the scale of Allred–Rochow)[13] of the X atoms as a function of q_h. The correlation is not bad since part of our hierarchy is related to this ordering (for instance $\chi_C > \chi_B > \chi_{Pb}$), but it is not total. Note however that electronegativities rather well reflect, in its literal sense, the XH_bX angles since Figure 2c has something of a mirror image of Figure 2b.

Since none of these factors entirely fits the proposed hierarchy, let us turn back to the oversimplified model of the XHX three-center bond and try to further develop it.

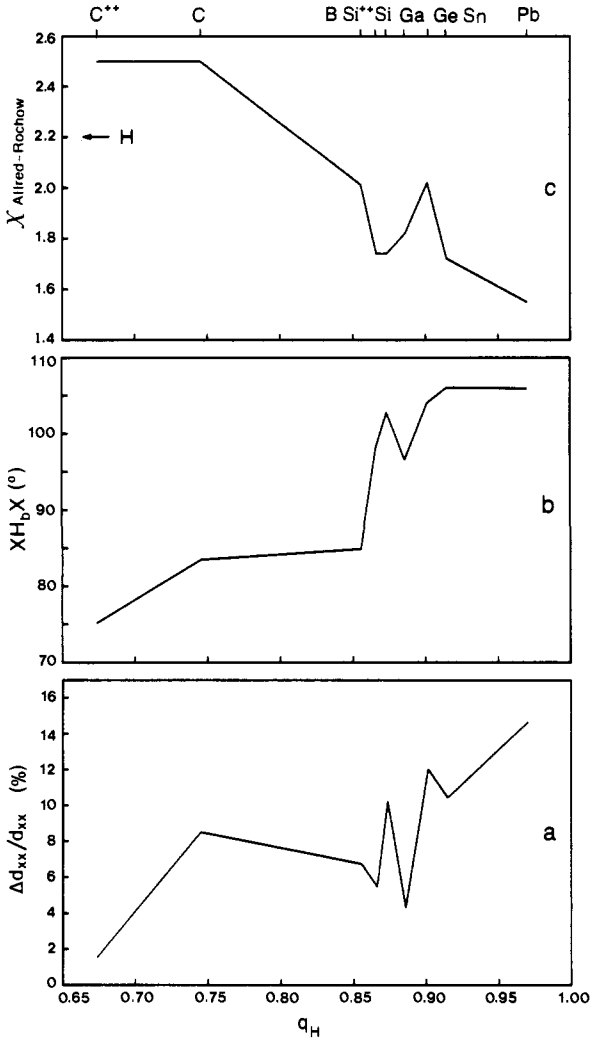

Figure 2. Correlations between the CASSCF-calculated charges on the bridging hydrogens and (a) the relative XX lengthenings with respect to typical single-bond lengths, (b) the XH_bX angles, and (c) the atomic electronegativities.

B. Back to an Elementary Model. In a simple Hückel picture, the bridge is defined in the basis of the three NAMOs b_1, b_2, and h (**10**). The wave function associated with this system has as

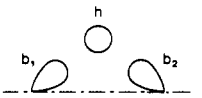

10

monoelectronic hamiltonian matrix elements the following matrix

	b_1	b_2	h
b_1	$\Delta\alpha$	β'	β
b_2	β'	$\Delta\alpha$	β
h	β	β	0

(1)

in which the diagonal elements $\Delta\alpha$ are the electronegativity differences between b and h and the off-diagonal elements β and β' are the integrals:

$$\beta = \langle b|h|h\rangle;\ \beta' = \langle b_1|h|b_2\rangle$$

This matrix can be reduced in two blocks, due to the symmetry of the system:

	$(b_1+b_2)/\sqrt{2}$	h	$(b_1-b_2)/\sqrt{2}$
$(b_1+b_2)/\sqrt{2}$	$\Delta\alpha+\beta'$	$\sqrt{2}\beta$	0
h	$\sqrt{2}\beta$	0	0
$(b_1-b_2)/\sqrt{2}$	0	0	$\Delta\alpha+\beta'$

(2)

(9) (a) For mixed compounds of boron and silicon, see: Mains, G. J.; Bock, C. W.; Trachtman, M. *J. Phys. Chem.* **1990**, *94*, 5449. (b) For aluminum–boron hydrides, see: Mains, G. J.; Bock, C. W.; Trachtman, M.; Finley, J.; McNamara, K.; Fisher, M.; Wociki, L. *J. Phys. Chem.* **1990**, *94*, 6996. Barone, V.; Minichino, C.; Lelj, F.; Russo, N. *Inorg. Chem.* **1981**, *20*, 1687. (c) For gallium–boron hydrides, see: Barone, V.; Minichino, C.; Lelj, F.; Russo, N. *J. Comput. Chem.* **1988**, *9*, 518. Duke, B. J.; Schaefer, H. F., III *J. Chem. Soc., Chem. Commun.* **1991**, 123. Pulham, C. R.; Brain, P. T.; Downs, A. J.; Rankin, D. W. H.; Robertson, H. E. *J. Chem. Soc., Chem. Commun.* **1990**, 177. Leszczynski, J.; Lammerstsma, K. *J. Phys. Chem.* **1991**, *95*, 3941.

(10) For a study on the *analogy between trivalent boron and divalent silicon*, see: Jemmis, E. D.; Prasad, B. V.; Tsuzuki, S.; Tanabe, K. *J. Phys. Chem.* **1990**, *94*, 5530. In this work, however, no mixed compound such as **9** with A = BR_2 and B = SiR was studied.

(11) One can further fine tune with the terminal substituents R.

(12) The typical singly bonded molecules are D_{2d} X_2H_4 for group 13 hydrides and D_{3d} X_2H_6 for group 14 hydrides. The corresponding SCF-DZP X–X distances (Å) are the following: B, 1.678; Ga, 2.530; C, 1.525; Si, 2.345; Ge, 2.497; Sn, 2.789; Pb, 2.837.

(13) Kahn, O.; Koenig, M. F. *Données fondamentales pour la chimie*; Hermann: Paris, 1972. Pauling's scale of electronegativity would give the same behavior.

Table V. Calculated Elements of the Fock Matrix on the Basis of NAMOs[a]

	$C_2H_6^{2+}$	C_2H_4	B_2H_6	$Si_2H_6^{2+}$	Si_2H_4	Ga_2H_6	Ge_2H_4	Sn_2H_4	Pb_2H_4
F_{b_1h}	−0.43	−0.41	−0.44	−0.41	−0.39	−0.36	−0.35	−0.33	−0.29
$F_{b_1b_2}$	−0.33	−0.25	−0.27	−0.23	−0.23	−0.23	−0.20	−0.22	−0.17
$F_{b_1h'}$	+0.08	+0.07	+0.02	+0.01	−0.01	−0.00	−0.01	−0.01	−0.01
$F_{b_1b'_2}$	−0.26	−0.21	−0.19	−0.11	−0.08	−0.08	−0.07	−0.05	−0.04
$F_{hh'}$	+0.08	+0.17	+0.11	+0.09	+0.10	+0.07	+0.09	+0.07	+0.06
$F_{b_1b'_1}$	−0.10	−0.08	−0.10	−0.12	−0.06	−0.09	−0.04	−0.04	−0.02
$F_{n_1n_2}$	−0.59	−0.46	−0.46	−0.34	−0.31	−0.32	−0.26	−0.27	−0.22
$F_{p_1p_2}$	−0.07	−0.04	−0.08	−0.12	−0.15	−0.15	−0.13	−0.17	−0.13
$F_{b_1b_1} - F_{hh}$[b]	−0.08	−0.03	+0.09	+0.07	+0.08	+0.11	+0.09	+0.13	+0.15

[a] In au, see **4** and **5** for orbital labeling. [b] This is $\Delta\alpha$, which translates the electronegativity differences.

Table VI. Some Ratios Calculated from Table V

	$C_2H_6^{2+}$	C_2H_4	B_2H_6	$Si_2H_6^{2+}$	Si_2H_4	Ga_2H_6	Ge_2H_4	Sn_2H_4	Pb_2H_4
$\Delta\alpha/\beta$	+0.19	+0.08	−0.20	−0.17	−0.22	−0.30	−0.27	−0.40	−0.51
β'/β	0.77	0.60	0.61	0.56	0.60	0.64	0.57	0.66	0.60
F_{inter}/F_{intra}[a]	0.48	0.47	0.33	0.28	0.21	0.22	0.20	0.18	0.15
$\beta/(\Delta\alpha + \beta')$	1.05	1.46	2.46	2.58	2.63	2.88	3.40	3.82	11.82
q_h(model)[b]	0.680	0.765	0.858	0.865	0.867	0.878	0.897	0.908	0.970
q_h(CASSCF)	0.674	0.745	0.856	0.866	0.874	0.886	0.902	0.915	0.970

[a] This ratio is defined as $(2|F_{b_1b'_2}| + 4|F_{b_1h'}| + 2|F_{b_1b'_1}| + |F_{hh'}|)/(4|F_{b_1h}| + 2|F_{b_1b_2}|)$. [b] Calculated from eq 5 and assuming independent bridges.

For a two-electron problem in its most general case, the occupied MO is symmetrical and may be written as

$$\varphi = ((b_1 + b_2)/\sqrt{2}) \cos\theta + h \sin\theta \qquad (3)$$

The associated energy is

$$\epsilon = \langle\varphi|h|\varphi\rangle$$

which may be written, using (2) and (3), as

$$\epsilon = (\Delta\alpha + \beta') \cos^2\theta + \beta\sqrt{2} \sin 2\theta$$

This energy is minimum for

$$d\epsilon/d\theta = 0$$

$$-(\Delta\alpha + \beta') \sin 2\theta + 2\beta\sqrt{2} \cos 2\theta = 0$$

$$\tan 2\theta = 2\sqrt{2}\frac{\beta}{\Delta\alpha + \beta'} \qquad (4)$$

From (3) and (4), the charge in orbital h is defined as

$$q_h = 2 \sin^2\theta$$

$$q_h = 2 \sin^2\left\{\frac{1}{2} \arctan\left(\frac{2\sqrt{2}\beta}{\Delta\alpha + \beta'}\right)\right\} \qquad (5)$$

q_h appears therefore governed by the ratio $\beta/(\Delta\alpha + \beta')$, which means that q_h is a function of both $\Delta\alpha/\beta$ and β'/β, these two ratios having analytically the same influence since (5) can also be written as

$$q_h = 2 \sin^2\left\{\frac{1}{2} \arctan\frac{2\sqrt{2}}{\frac{\Delta\alpha}{\beta} + \frac{\beta'}{\beta}}\right\} \qquad (6)$$

One may also analytically express the CORP index between b_1 and b_2 in the three-center problem as a simple polynomial of q_h.[14] From (6) we have therefore

$$\mathrm{CORP}(b_1,b_2) = f\left(\frac{\Delta\alpha}{\beta}, \frac{\beta'}{\beta}\right) \qquad (7)$$

Both eqs 6 and 7 show that the regular changes of q_h and $\mathrm{CORP}(b_1,b_2)$ observed along the series cannot unequivocally be interpreted as a signature of the single through-space vs through-bond ratio β'/β, since they may be strongly influenced by the changes in the electronegativity of the heavy atoms as well. The rather poor correlation observed in Figure 2c should not exclude that electronegativity difference is the leading factor since in our model $\Delta\alpha$ is the difference between the energy of the *hybridized* b orbital and that of the hydrogen orbital. The b NAMOs correspond to hybrids with s and p mixtures, while conventional atomic scales of electronegativity concern the most external atomic orbitals. Moreover, the XH interaction term β may vary significantly from one compound to another so that the ratio $\Delta\alpha/\beta$ may not follow the simple parameter $\Delta\alpha$.

In order to discriminate the leading factor in the observed changes of the wave functions, and to understand the interplay of the various factors, it appears therefore necessary to evaluate each of these matrix elements α and β. In our OVB calculations, these transfer integrals correspond to the Fock matrix elements on the basis of the NAMOs. In other words, the ab initio evaluations of β, β', and $\Delta\alpha$ are given respectively by the elements

$$F_{bh} = \langle b_1|F|h\rangle$$

$$F_{b_1b_2} = \langle b_1|F|b_2\rangle$$

$$F_{bb} - F_{hh} = \langle b_1|F|b_1\rangle - \langle h|F|h\rangle$$

C. Use of the *F* Transfer Integrals. The calculated Fock operator is relative to the closed-shell configuration $\Phi_0 = |a_g^2 b_{(1)u}^2|$ which is the dominant part in our CASSCF wave functions ($C_0 \approx 0.98$).[15] The diagonal elements F_{bb} and F_{hh} will be used to calculate $\Delta\alpha$ and the off-diagonal elements F_{ij} will be used to calculate β and β'. These elements F_{ij}, which are the hopping integrals of the solid-state physicist, are especially apt to analyze the importance of the charge transfers between the upper and lower bridges, as well as to estimate the through-space/through-bond bonding ratios.

The Fock matrix elements are listed in Table V. Some interesting ratios and further processing of these values are listed in Table VI. Concerning the diagonal elements F_{ii}, only the differences $(F_{b_ib_i} - F_{hh})$ are relevant and will furnish the terms $\Delta\alpha$ associated with the electronegativity differences. Concerning the off-diagonal elements F_{ij}, these are a measure of the charge transfers between the NAMOs. They are used to estimate the

(14) See Appendix, Section 2.

(15) This procedure was already suggested in ref 4. In that work, however, the F_{ij} hopping integrals for B_2H_6 were evaluated from the CI matrix elements in the OVB determinant basis. This gives smaller amplitudes but about similar ratios (for instance, $F_{b_1b_2}/F_{b_1h} = 0.59$ instead of 0.61 in the present work).

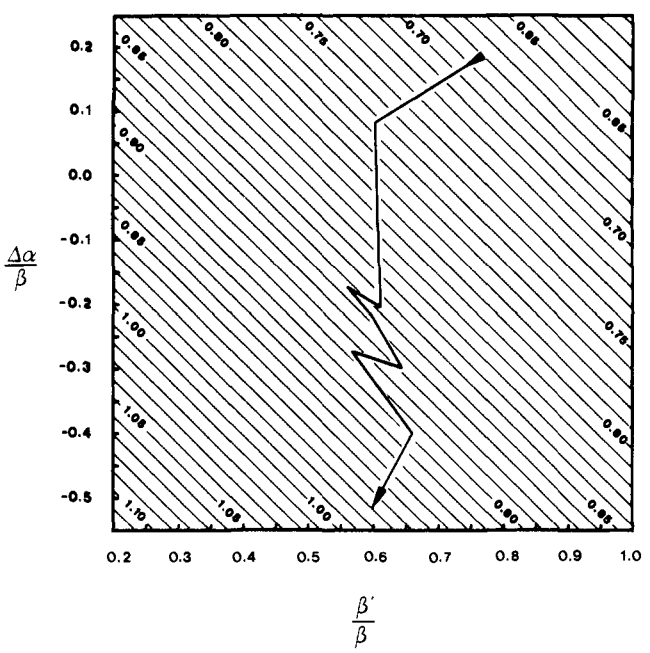

Figure 3. Two-dimensional map of q_h against β'/β and $\Delta\alpha/\beta$, calculated according to eq 6. The isocharge curves are separated by 0.01 e, starting from 0.60 (top right) and ascending to 1.12 (bottom left). The location of the studied compounds on this surface is indicated by the broken path from $C_2H_6^{2+}$ (top) to Pb_2H_4 (bottom).

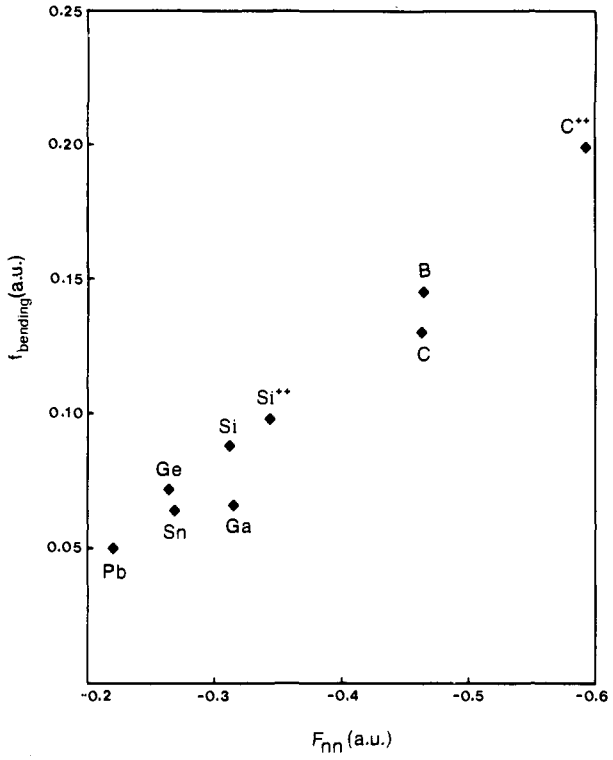

Figure 4. Correlation between the bending force constants and the $F_{n_1n_2}$ Fock matrix elements.

β'/β ratio and to analyze the importance of the global charge transfers between the two bridges—another measure of their independence. The main results of Tables V and VI can be analyzed as follows:

(1) On the basis of the X–H directed NAMOs ({b,h} set, 4), the F_{bh} element is always the largest one. In the X–X directed basis ({n,p} set, **5**), the $F_{n_1n_2}$ elements, which are the simple sums $F_{b_1b_2} + F_{b_1b'2}$, may reach rather strong values so that for $C_2H_6^{2+}$, C_2H_4, and B_2H_6 we have $|F_{n_1n_2}| > |F_{bh}|$. One should not forget, however, that there are four b–h interactions while the n–n one is single.

(2) Among the four interbridge elements, $F_{b_1h'}$ is either positive or negligible while $F_{hh'}$ is always positive. This supports the antibonding character of the $H_b\cdots H_b$ interaction in any compound of the series. $F_{b_1b'_2}$ is the largest interbridge element and regularly decreases along the series from $C_2H_6^{2+}$ to Pb_2H_4. The ratio of all interbridge over intrabridge interactions (F_{inter}/F_{intra} in Table VI) can be considered as a measure of the relative importance of the intrabridge vs interbridge interactions. This ratio correlates rather well with the calculated probability of finding 2 electrons in one bridge ($P^{(2)}_{b_1,h,b_2}$ in Table II), thus confirming the trend to more separate bridges from $C_2H_6^{2+}$ to Pb_2H_4.

(3) The strongest charge transfer elements, intrabridge F_{b_1h} and $F_{b_1b_2}$, have decreasing amplitudes along the series. This is in agreement with the X–H bond being stronger in B_2H_6 than in its heavier analogue Al_2H_6,[9b] but we will reconsider this point later when addressing the dimerization energies.

(4) The through-space/through-bond ratio β'/β, measured by the ratio $F_{b_1b_2}/F_{b_1h}$, is rather constant along the series (β'/β = 60 ± 5%), except for $C_2H_6^{2+}$ where all direct C–C interactions are strong. This indicates that the observed diminution of q_h and CORP(b_1–b_2) along the series cannot be attributed to a decrease of the through-space vs through-bond interactions. In other words, except for $C_2H_6^{2+}$, *the electronic channels have comparable relative widths in all bridges.*

(5) The orbital energy differences exhibit changes of large amplitude along the series. As expected, $\Delta\alpha$ changes its sign between C and B. The ratio $\Delta\alpha/\beta$ varies from −0.51 to +0.19. This variation is 10 times larger than that of the β'/β ratio, so that *the orbital electronegativity appears as the main factor of the changes in the electronic wave function.*

Reporting the $\Delta\alpha/\beta$ and β'/β ratios of Table VI, evaluated from the F elements, in eq 6 gives theoretical charges q_h corresponding to a treatment of isolated bridges, i.e. omitting the charge transfers between the two bridges. These theoretical charges are given in Table VI (q_h(model)) and are compared to the exact ones (q_h(CASSCF)). Both happen to be quite close (within 1%, except for C_2H_4 where q_h(model) is larger than q_h(CASSCF) by 3%) which again supports strong independence of the bridges and shows the relevance of the modeling in terms of the two ratios.

The relative involvement of the two parameters of eq 6 along our series is visualized in Figure 3. This is a 2-D map of theoretical q_h as a function of β'/β (x axis) and $\Delta\alpha/\beta$ (y axis). Because of the equivalent role of these two parameters in eq 6, the isocharge curves are 45°-sloped parallel straight lines. The q_h function monotonously decreases from bottom left to top right. The curves correspond to regular variations of q_h (0.01 e). Since these lines appear rather equidistant in the map, the shape of the q_h surface is therefore not far from planarity. We have next reported in Figure 3 the location of our nine compounds using the parameters of Table VI. Walking along the path from $C_2H_6^{2+}$ (top) to Pb_2H_4 (bottom), one climbs continuously toward higher q_h but using a rather sinuous trail. This translates the non-monotonous variations of both parameters along our scaling, as seen in Table VI. Figure 3 clearly shows the relative extent of the two parameters. Little displacement is made along the x axis (β'/β ratio fairly constant) whereas the hill is climbed mainly along the y axis (wide changes of the $\Delta\alpha/\beta$ ratio). This illustrates how q_h is governed more by the electronegativity factors than by the through-space/through-bond binding ratio. The unique exception is $C_2H_6^{2+}$ which has a β'/β ratio significantly larger than that of the other members. Note in Figure 3 that each point of the pathway is lying exactly on the q_h surface as long as q_h is calculated from the model. Taking the exact CASSCF-calculated q_h would locate these points either slightly below the analytical surface ($C_2H_6^{2+}$, C_2H_4, and B_2H_6) or slightly above it (remaining systems).

In Table VI is also given the ratio $r = \beta/(\Delta\alpha + \beta')$ to show its regular variation across the series. The function $q_h = f(r)$ given by eq 5 increases monotonously from 0 to 1 when r varies from 0 to $+\infty$ and from 1 to 2 when r varies from $-\infty$ to 0.[16]

Table VII. Decomposition of the SCF Dimerization Energies (kcal/mol)

	BH_3	GaH_3	CH_2	SiH_2	GeH_2	SnH_2	PbH_2
monomer deformation	38.9	29.7	11.6	7.3	8.9	7.3	8.7
electrostatic	−29.3	−32.2	−38.9	−28.6	−18.9	−29.6	−32.7
repulsion	119.9	73.6	245.4	108.3	92.7	74.8	65.8
delocalization	−150.7	−85.5	−224.9	−114.0	−106.7	−85.7	−72.5
total SCF	−21.2	−14.4	−6.8	−26.9	−24.0	−33.3	−30.6

The F_{nn} elements can also be expected to parallel the force constants associated to the pure in-plane bending of the X_2H_{b2} rings—the symmetrical deformation maintaining global a_g symmetry and keeping all X–H distances unchanged. From the symmetrized Cartesian force constant matrices, it is possible to isolate the specific contributions of such special coordinates by making a cross section in the normal mode hypersurface. As can be seen in Figure 4, these $f_{bending}$ (or f_{xx}) elements approximately follow the corresponding F_{nn} Fock matrix integrals. In other words, the hardness of the X⋯X spring may reasonably be related to the width of the electronic XX channel.

D. Peculiarity of $C_2H_6^{2+}$ and the Diprotonation of X_2H_4. From the above discussion, and in particular regarding the β'/β ratio, $C_2H_6^{2+}$ seems to be the only species in which strong CC binding is maintained. This singularity would be better evidenced by comparing $C_2H_6^{2+}$ with its heavier analogue $Si_2H_6^{2+}$. Both species can be seen as the dications of ethane and disilane respectively or as the diprotonation products of ethylene and disilene. In this case, two forms can be protonated: that with the X=X double bond[17] or that with the X–H–X double bridge. Although somewhat academic, the following question will serve as a guideline in our comparison: Is $X_2H_6^{2+}$ better seen as the diprotonation product of a double bond or of a double bridge?

When the planar double bond is diprotonated,[18] the two protons are expected to approach from either side of the plane, in the middle of the X=X axis, **11**. They stick to the π cloud, which

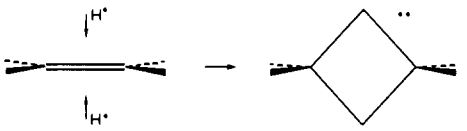

11

rearranges through $\sigma + \pi$ mixing into the two symmetrical three-center two-electron bridges. Writing the double bond as two banana bonds would prepare and anticipate the double bridge. In this case, the protons approach toward the middle of each banana bond and stabilize the electronic pairs, which before only used the sp^3-type hybrids on each X atom. In such a scheme, the diprotonation brings little change to the structure of the molecule. This can be illustrated by the similar shapes of the contour lines for localized orbitals obtained from the banana bonds in ethylene or from typical three-center two-electron bonds in diborane.

When the double bridge is diprotonated, the two protons just cling to the extracyclic lone pairs, **12**. Due to their nonbonding

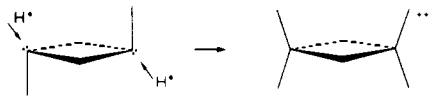

12

character, the starting structure should maintain a double bridge unaffected by the diprotonation.[19] An even larger structural similarity is thus expected for doubly bridged X_2H_4 and $X_2H_6^{2+}$. To bring out the similarities and differences in our two pairs of compounds, let us use the results on geometry, proton affinity, and electronic structure.

The electronic indexes $P^{(2)}$, CORP, and F all indicate that when going from doubly bonded $H_2Si{=}SiH_2$ to doubly bridged $Si_2H_6^{2+}$, much of the Si=Si double link is destroyed, while much of the C=C double link is maintained when going from doubly bonded $H_2C{=}CH_2$ to doubly bridged $C_2H_6^{2+}$. As explained in Section 3 in the Appendix, examination of the geometries and proton affinities leads to similar trends. Geometry, energy, and wave function arguments therefore suggest that $C_2H_6^{2+}$ in its D_{2h} form is better seen as symmetrically diprotonated doubly bonded ethylene, while D_{2h} $Si_2H_6^{2+}$ is better seen as symmetrically diprotonated doubly bridged Si_2H_4. In other words, the unsaturated neutral form which survives better in the dication is the double bond for $C_2H_6^{2+}$ and the double bridge for $Si_2H_6^{2+}$. For carbon, this logically follows from a very unfavored bridged form for C_2H_4 (not a true minimum, high in energy). For silicon, this result is more interesting since the bridged form of Si_2H_4, although a true minimum, low in energy, is still above the double-bonded form.

V. Dimerization Energies

The energy of dimerization of two RXH fragments into a double bridge is a measure of its stability. For the group 14 XH_2 fragments, such dimerization energy was found to be roughly constant whatever X.[3] To understand what it is made of, let us partition the SCF-calculated dimerization energy into its four basic components, as is done for intermolecular problems:[20-22] (1) A deformation energy is first necessary to bring each fragment XH_n to its geometry in the dimer. (2) An electrostatic term is the classical electrostatic energy between the two electron–nuclei charge distributions of the two partners A and B. Once the fragments are brought to the dimer geometry, this energy term can be written

$$E_{elec} = \langle \Phi_A \cdot \Phi_B | H | \Phi_A \cdot \Phi_B \rangle$$

where each member of the integral is the simple product, without antisymmetrization, of the SCF wave functions Φ_A and Φ_B of the two deformed fragments. (3) Next, we add a repulsion energy due to the exclusion principle and brought by the antisymmetrization

$$E_{rep} = \langle |\Phi_A \Phi_B| | H | | \Phi_A \Phi_B| \rangle - \langle \Phi_A \cdot \Phi_B | H | \Phi_A \cdot \Phi_B \rangle$$

(16) In effect, when $\beta/(\Delta\alpha + \beta') < 0$ the physically relevant solution for eq 4 is

$$\theta = \frac{\pi}{2} - \arctan \frac{2\sqrt{2}\beta}{\Delta\alpha + \beta'}$$

so that eq 5 now becomes

$$q_h = 2 \sin^2 \left\{ \frac{\pi}{2} + \frac{1}{2} \arctan \frac{2\sqrt{2}\beta}{\Delta\alpha + \beta'} \right\}$$

(17) The analogy between diborane and a protonated double bond was noticed long ago: Pitzer, K. *J. Am. Chem. Soc.* **1945**, *67*, 1126.

(18) Disilene is found to be planar at the SCF level. At a refined level, it is found to be trans bent with a very weak barrier to planarity between the two trans-bent forms (~1 kcal/mol). So, disilene can be considered as virtually planar. In the diprotonation of a trans-bent double bond, the protons no longer arrive at the middle of X=X, but the system restores full D_{2h} symmetry in order to minimize the repulsion between the six hydrogens.

(19) In the X_2H_4 series with X = Si, Ge, Sn, Pb the two doubly bridged isomers, cis and trans, are nearly degenerate in energy and structure. The present discussion therefore holds for both isomers. It would no longer hold for cis-bridged C_2H_4 which has a peculiar structure, as discussed in ref 3.

(20) Morokuma, K. *J. Chem. Phys.* **1971**, *55*, 1236.

(21) Dreyfus, M.; Pullman, A. *Theor. Chim. Acta* **1970**, *19*, 20.

(22) Kollman, P. A.; Allen, L. C. *Theor. Chim. Acta* **1970**, *18*, 399.

(4) Last, the delocalization energy leads to the final SCF energy

$$E_{del} = \langle \Phi_{AB}|H|\Phi_{AB}| \rangle - \langle |\Phi_A\Phi_B||H||\Phi_A\Phi_B| \rangle$$

Discarding the cases of the dications for which the dimerization energy does not make much sense, all these contributions are listed in Table VII.

The deformation energies are necessarily positive. The deformation consists of a stretching of one X–H bond (by about 10%) and of an angular HXH variation. The energy loss due to the stretching is expected to be roughly proportional to the force constant and to the X–H bond energy, which explains the differences between the first row and following row compounds (B vs Ga, C vs Si). The angular deformation is of course negligible for the XH_2 fragments while it is quite considerable for the XH_3 fragments which change from a planar geometry to a strongly pyramidal arrangement. This accounts for the large differences between B, Ga and C, Si, Ge, Sn, Pb in the deformation energies of Table VII.

Electrostatic energies here correspond essentially to the attractive interactions between the two bond dipoles of the lengthened $X-H_b$ bonds engaged in the bridges. This term mainly depends on the XH bond polarity and on the distance between the bonds Noticing that the Mulliken net charges on H_b and X were quite close in the monomer and in the dimer, we have proposed elsewhere a simplified expression of the electrostatic energy based on single point charges.[3] The actual electrostatic energies reported in Table VII are not that far from this crude model. They are fairly close to each other (around 30 kcal/mol) and to the final SCF dimerization energies, except for C_2H_4 (but remember this bridge is not a real minimum).

The repulsive energies depend on the overlap between the X–H bond orbitals. These become more and more diffuse for heavier elements. The trend appears regular in Table VII although this effect is partly counterbalanced by the increase in interatomic distances.

The delocalization energies should follow the Fock matrix elements (mainly F_{b_1-h}) and decrease along the series. This appears in Table VII. The delocalization and repulsion energies compensate each other along the series, which solves the apparent paradox between the rather constant dimerization energies for CH_2 to PbH_2[3] and the consistent decrease of the corresponding F_{ij} off-diagonal elements. Their amplitudes range fairly well within our scale (only GaH_3 is not exactly in the right place but it is not far from it). Except for the case of CH_2, there is about −10 kcal/mol more delocalization than repulsion. For X_2H_4 compounds, this roughly compensates the fragment deformations so that the final SCF dimerization energies roughly follow the electrostatic contributions. For BH_3 and GaH_3, the interplay is slightly different. For BH_3, the delocalization contribution overcompensate the repulsion by as much as −30 kcal/mol, but this is in turn compensated by the largest fragment deformation energy (+39 kcal/mol). For GaH_3, the large fragment deformation energy is mainly responsible for the reduced final SCF dimerization energy. For CH_2, the repulsion energy overcompensates the delocalization energy by as much as +20 kcal/mol, and this is responsible for an even more reduced SCF dimerization energy. In the results reported in Table VII, the C_2H_4 compound exhibits very large repulsion and delocalization terms. This may be due both to the nature of the carbon hybrid orbitals and to the rather short C–C distance.

The effect of electronic correlation on the dimerization energies of XH_2 has been discussed elsewhere.[3] That on the dimerization of BH_3 is well-documented.[23,24] We have calculated the MP2 corrections for the dimerization energies of BH_3 and GaH_3. We found −40.4 and −23.3 kcal/mol, respectively, both SCF and MP2 results being in excellent agreement with the calculations by Lammerstsma and Leszczynski.[7a] In that work, MP4 refinements bring little change to these values while our configuration interaction calculations performed with the CIPSI algorithm[25] reduce these values by 7–8 kcal/mol.

Table VIII. OVB Results on the Singly Bridged Forms[a]

		Sn_2H_4	Pb_2H_4
NAMO populations	b_1	0.46	0.52
	h	1.01	1.07
	b_2	0.53	0.42
	c_1	0.87	0.69
	c_2	1.13	1.31
	$\{c_1,c_2\}$	2.00	1.99
	$\{b_1,h\}$	1.47	1.59
	$\{b_2,h\}$	1.54	1.48
$P^{(2)}$	$\{b_1,h\}$	50.6	60.7
	$\{b_2,h\}$	56.6	51.6
	$\{b_1,b_2\}$	19.5	15.9
	$\{c_1,c_2\}$[b]	99.5	99.2
	$\{b_1,c_2\}$	37.6	40.3
	$\{c_1,b_2\}$	35.0	26.1
CORP	b_1-h	14.3	21.2
	b_2-h	18.2	14.6
	b_1-b_2	−2.6	−4.2
	c_1-c_2	52.1	54.1
	b_1-h-b_2	61.5	60.6
	b_1-c_2	−2.2	−3.9
	c_1-b_2	−0.7	0.6

[a] See **14** for orbital labeling. $P^{(2)}$ and CORP in percent. [b] Same as $\{b_1,h,b_2\}$.

VI. Comparison with Single Bridges

An OVB analysis has been performed on the singly bridged systems **13** found to be local minima for Sn_2H_4 and Pb_2H_4. Only partial results were given in a previous work,[26] and we would like to report here more completely the results concerning the NAMO populations, the $P^{(2)}$ probabilities, and the CORP indexes. In particular, it is interesting to test this last index for such peculiar

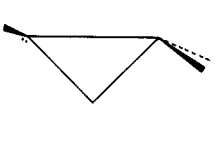

13

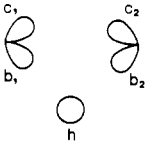

14

XX bonds. The corresponding NAMOs are labeled in **14**. In such a structure, there are basically two well-separated bonds: a three-center two-electron bridge (b_1-h-b_2) and a two-center two-electron bond (c_1-c_2), the nature of which is between covalent and dative according to the two possible limiting views of the bonding $H\ddot{X}-XH_3$ (**15**) or $H_2X\leftarrow:XH_2$ (**16**). The results of the

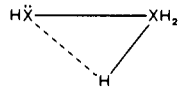

15

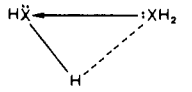

16

OVB treatments are given in Table VIII. As noticed elsewhere,[26] the separation between the two bonds is nearly complete. The formal distribution of the electron pairs in the bridges is no longer symmetrical and the population in the h NAMO on the bridging hydrogen is now larger than 1e for both compounds. Although one is still close to the allylic-type distribution $^1/_2,1,^1/_2$, these bridges are located beyond Pb_2H_4 in our scale. According to our model, the two factors equally responsible for the q_h population are β'/β and $\Delta\alpha/\beta$. Since in both compounds the X–X distances are much shorter here than in the double bridges, one expects a larger β'/β ratio which should induce a smaller population in the h NAMO. The opposite effect is observed, indicating that the

(23) Ortiz, J. V.; Lipscomb, W. N. *Chem. Phys. Lett.* **1983**, *103*, 59.
(24) Barone, V.; Minichino, C. *Theor. Chim. Acta* **1989**, *6*, 53.
(25) Huron, B.; Malrieu, J. P.; Rancurel, P. *J. Chem. Phys.* **1973**, *58*, 5745.
(26) Trinquier, G. *J. Am. Chem. Soc.* **1991**, *113*, 144.

$\Delta\alpha/\beta$ term is the driving force for the high q_h charge. Although the atoms are identical in the doubly bridged and singly bridged systems, electronegativity factors make the difference between them. This again emphasizes that it is the electronegativity of the *orbitals* (b_1,h,b_2) that is involved: although the X–H–X atoms are identical, the nature and the environment of the b_1,h,b_2 orbitals are different in both systems.

A marked dissymmetry occurs in the b_1–h–b_2 bridges of the singly bridged molecules. Comparison of the $P^{(2)}$ probabilities in Tables II and VIII as well as the CORP indexes in Tables III and VIII enables us to compare the b–h bonds in the doubly bridged systems with the b_1–h and h–b_2 bonds in the singly bridged systems. In Sn_2H_4, going from the symmetrical doubly bridged isomer to the unsymmetrical singly bridged one, the b_1–h bond remains unchanged while the h–b_2 bond is significantly strengthened. The opposite occurs in Pb_2H_4 where b_1–h is strengthened whereas h–b_2 remains unchanged. This also follows the corresponding bond lengths[26] and suggests that Sn_2H_4 is closer to **15** while Pb_2H_4 is closer to **16**. Note that the total electron population in the b–h set which is strengthened should be increased (from 1.5e up to 2e in a schematic limiting case), so that the population in the opposite b orbital is expected to decrease. This is confirmed in Table VIII, which shows that the opposite b orbital actually loses electron charge to the benefit of the h NAMO, which goes beyond 1e, while the b orbital of the strengthened b–h bond remains unchanged with respect to the doubly bridge situation.

The populations in orbitals c_1 and c_2 are fairly close to 1e, especially for Sn_2H_4, suggesting a c_1–c_2 bond close to a homopolar two-center two-electron bond. One notices in Table VIII strong CORP indexes for these bonds. Regardless of the initial nature—covalent or dative—of a two-center two-electron bond, its associated CORP index can be analytically expressed from the electronic population q in one of the two orbitals.[14] From such an uncorrelated model, and using the c_1 populations of Table VIII, the theoretical CORP indexes for c_1–c_2 are calculated at 62.1% for Sn_2H_4 and 59.7% for Pb_2H_4, which is above the NAMO + OVB values. For these last indexes, there is an apparent paradox since Sn–Sn, which should be stronger and more covalent than Pb–Pb, has the smaller CORP index (52% vs 54%). This is due to the electronic correlation in the c_1–c_2 bond, stronger in Sn_2H_4 than in Pb_2H_4, as shown in ref 26.[27] One will remember, however, that both CORP indexes for c_1–c_2 are large, supporting strong X–X bonds.

An interesting point about the singly bridged structures is that they can be seen as a precursor of the ethyl cation $C_2H_5^+$ in its most stable C_{2v} bridged from.[28] Again, this cation is obtained by the protonation of an extracyclic lone pair, **17**, which should

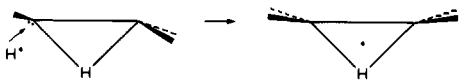

17

leave the X_2H bridge unaffected. Note, however, that in $C_2H_5^+$ the terminal hydrogens are slightly tilted away from the bridging hydrogen. The protonation, indeed, restores a symmetry between the four terminal hydrogens and enhances the positive charge on all of them. The tilting of the terminal hydrogens off the bridging hydrogen thus simply ensues from electrostatic arguments. With more strongly electropositive X atoms, the bridging hydrogen should participate little to the positive charge sharing, as discussed above for $Si_2H_6^{2+}$, so that in the heavier $X_2H_5^+$ cations, a tilting of the terminal hydrogens toward the bridged one is expected. This is confirmed in $Si_2H_5^+$,[29] as well as in all the heavier analogues.

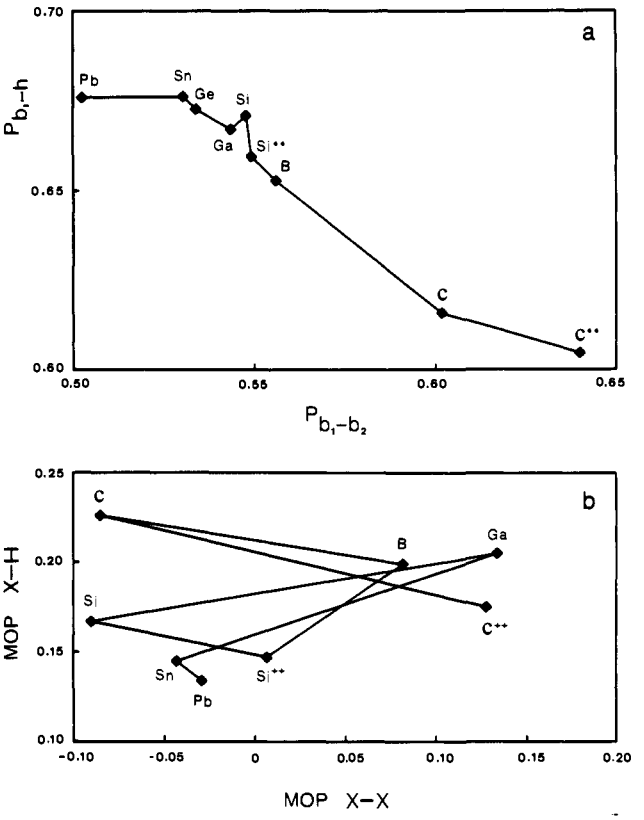

Figure 5. (a) b_1–h vs b_1–b_2 off-diagonal elements of the zero-order density matrix of the CASSCF wave functions expressed in the NAMO basis; (b) X–H vs X–X Mulliken overlap populations calculated from the SCF wave functions.

VII. Summary and Conclusion

The procedure based on the OVB decomposition of a CASSCF wave function, reexpressed in terms of NAMOs, enabled us to draw up some hierarchy in the electron-deficient double bridges. The main factors giving rise to consistent trends are (1) the separation of the bridges and (2) the relative importance of peripheral X–H–X bonding versus central X–X bonding. Only $C_2H_6^{2+}$ has exceptionally eminent central bonding. All other species exhibit primacy of peripheral bonding,[30] although to different extents. The trend may be evidenced by simply expressing the CASSCF wave function in terms of NAMOs, without performing the OVB decomposition. This is illustrated in Figure 5a which displays the b–h vs b_1–b_2 off-diagonal elements of the corresponding zero-order density matrix. It is to be noted that the simple SCF Mulliken overlap populations between X–H and X–X fail to evidence any consistent ordering, as shown in Figure 5b. Regarding the electronic structures, the observable which undergoes consistent and wide variations happens to be the formal population on the bridging hydrogen q_h. This parameter was used to define a scale. The ranging of the double bridges along this scale follows the two factors mentioned above. It is ultimately governed by the interplay between the through-bond/through-

(27) Correlation effects enhance the $P^{(1)}P^{(1)}$ term entering the definition of CORP and reduce it. The four components defining the index are as follows (in the c_1, c_2 ordering and in percent).

	Sn	Pb
$P^{(2)}$	99.5	99.2
$P^{(0)}P^{(2)}$	6.2	14.5
$P^{(1)}P^{(1)}$	39.7	30.1
$P^{(2)}P^{(0)}$	1.5	0.5
CORP	52.1	54.1

The $P^{(1)}P^{(1)}$ term is 10% larger for Sn than for Pb. This overcompensates the $P^{(0)}P^{(2)}$ term which is 8% larger for Pb than for Sn and which illustrates the better relevance of **16** for Pb_2H_4.

(28) (a) Raghavachari, K.; Whiteside, R. A.; Pople, J. A.; Schleyer, P. v. R. *J. Am. Chem. Soc.* **1981**, *103*, 5649. (b) Hehre, W. J.; Radom, L.; Schleyer, P. v. R.; Pople, J. A. *Ab initio Molecular Orbital Theory*; John Wiley and Sons: New York, 1986; p 384.

(29) Köhler, H.-J.; Lischka, H. *Chem. Phys. Lett.* **1983**, *98*, 454. Raghavachari, K. *J. Chem. Phys.* **1990**, *92*, 452.

(30) In agreement with other theoretical studies: Bader, R. F. W.; Essén, H. *J. Chem. Phys.* **1984**, *80*, 1943.

Table IX. SCF-Optimized Geometries for X_2H_6 Species[a]

	B_2H_6	Ga_2H_6	$C_2H_6^{2+}$	$Si_2H_6^{2+}$
$X-H_b$	1.327	1.768	1.284	1.634
$X-H_t$	1.195	1.549	1.099	1.455
X-X	1.791	2.639	1.549	2.473
H_bXH_b	95.1	83.5	105.8	81.7
XH_bX	84.9	96.5	75.2	98.3
H_tXH_t	122.3	129.1	121.8	136.3

[a] In anströms and degrees. The structures have D_{2h} symmetry. H_b and H_t refer to the bridging and terminal (i.e. extracyclic) hydrogens, respectively.

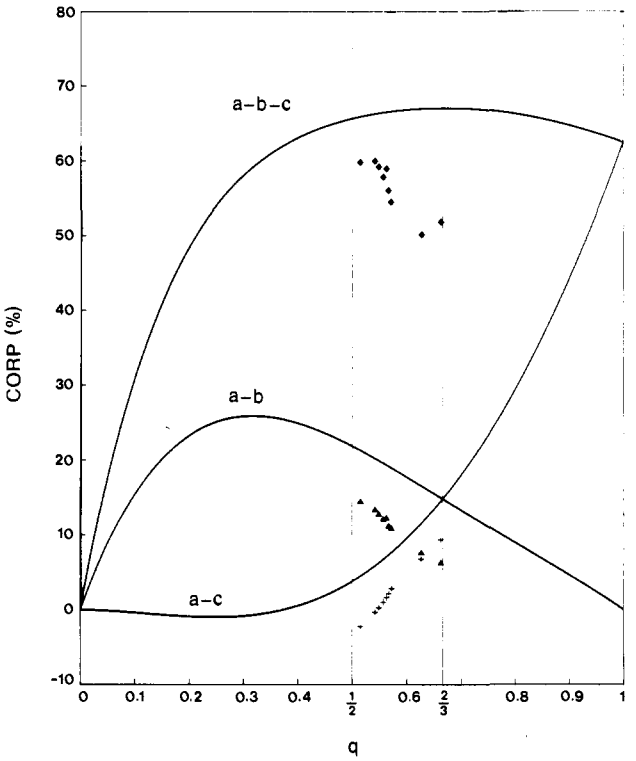

Figure 6. Theoretical CORP curves for a symmetrical three-center two-electron system a–b–c in an uncorrelated description. q is the electron population in a and c. Actual values for the double bridges are plotted for comparison (▲, b–h; +, b_1–b_2; ◆, b_1–h–b_2).

space ratio and an electronegativity factor which is the main driving force. The variations of the recently proposed CORP index[4] do not therefore reflect binding changes alone since the index is strongly correlated with the charges, and its use as a structural diagnosis should be essentially relevant in weakly polar (e.g. homonuclear) buildings.

As the electron densities on q_h can be indirectly accessed through the shielding constants and ^1H NMR chemical shifts, both testing of our proposed ordering and locating the other compounds in the scale could be achieved by using their relative ^1H_b chemical shifts under constant experimental conditions of solvent, concentration, and temperature. Compounds with unshielded bridging protons would be located on the left-hand side of the scale ($C_2H_6^{2+}$) while those with shielded bridging protons would occur on the right-hand side of it (Pb_2H_4).

The present analysis should be valid for all types of electron-deficient double bridges, regardless of the extracyclic saturation, such as those in group 13 X_2H_4[7b,31-33] or X_2H_2.[34] It should also remain valid for singly bridged or multiply bridged systems. The independence of the bridges explains why the X–H–X building block may enter the composition of singly, doubly, or multiply bridged compounds. This can be extended to bridged structures in transition-metal chemistry, where an isolobal fragment may replace either X (e.g. d^7 C_{2v} ML_4 —○— BH_2)[35] or H_b (e.g. d^7 ML_5 —○— H).[36] We also suggest the possible existence of mixed

Table X. SCF-Calculated Harmonic Vibrational Frequencies (cm^{-1})

		B_2H_6	Ga_2H_6	$C_2H_6^{2+}$	$Si_2H_6^{2+}$
a_g	ν_1	2723	2053	3148	2401
	ν_2	2268	1555	2223	1864
	ν_3	1285	819	1537	945
	ν_4	821	235	976	462
a_u	ν_5	875	476	1121	555
b_{1g}	ν_6	1895	1312	1934	1602
	ν_7	887	348	1046	480
b_{1u}	ν_8	2809	2039	3281	2482
	ν_9	1100	881	1049	1066
	ν_{10}	422	259	269	346
b_{2g}	ν_{11}	2793	2033	3287	2480
	ν_{12}	987	516	1265	657
b_{2u}	ν_{13}	2046	1228	2304	1612
	ν_{14}	1059	703	1282	801
b_{3g}	ν_{15}	1159	824	1166	989
b_{3u}	ν_{16}	2700	2046	3135	2401
	ν_{17}	1797	1394	1509	1725
	ν_{18}	1264	752	1227	877

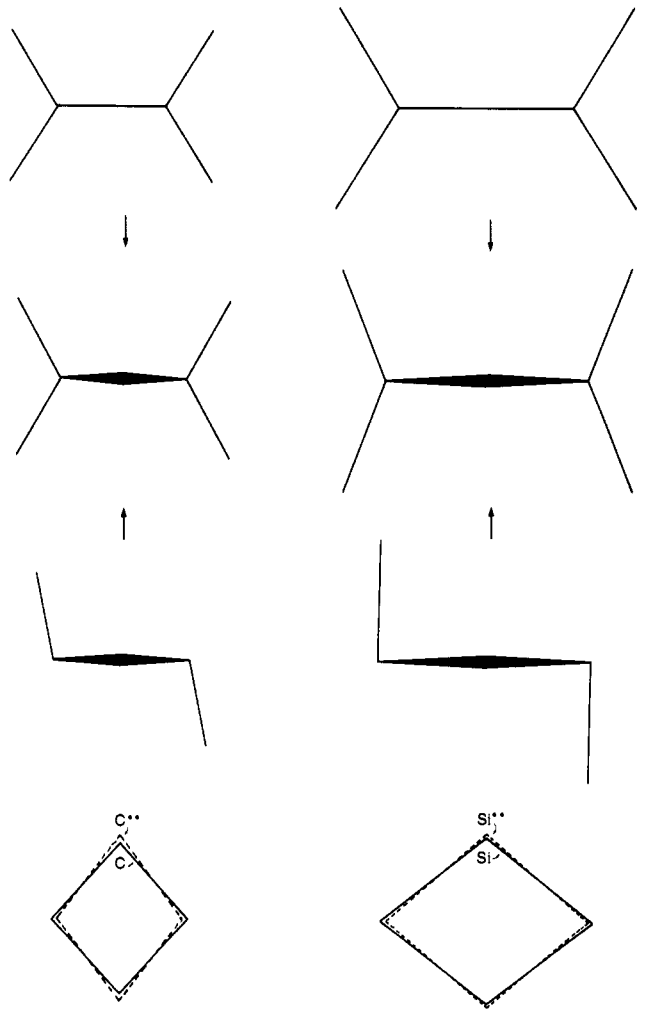

Figure 7. Geometries of X_2H_4 and $X_2H_6^{2+}$ for X = C (left) and X = Si (right). From top to bottom: doubly bonded X_2H_4, $X_2H_6^{2+}$, doubly bridged X_2H_4, and the bridge planes in both X_2H_4 and $X_2H_6^{2+}$.

(31) Curtiss, L. A.; Pople, J. A. *J. Chem. Phys.* **1989**, *90*, 4314.
(32) Ruscic, B.; Schwarz, M.; Berkowitz, J. *J. Chem. Phys.* **1989**, *91*, 4576.
(33) Slanina, Z. *J. Phys. Chem.* **1991**, *91*, 1089.
(34) Janiak, C.; Hoffmann, R. *J. Am. Chem. Soc.* **1990**, *112*, 5924.
(35) Masciocchi, N.; Sironi, A.; D'Alfonso, G. *J. Am. Chem. Soc.* **1990**, *112*, 9395.

Table XI. Calculated Diproton Affinities for C_2H_4 and Si_2H_4[a]

		C_2H_4	Si_2H_4
double bond	SCF	133.5	266.6
	CI[b]	129.0	259.2
	+ΔZPE[c]	117.5	246.2
double bridge	SCF	300.4	289.3
	CI	293.9	281.8
	+ΔZPE		269.3

[a] Defined as $E(X_2H_4) - E(X_2H_6^{2+})$, in kcal/mol. [b] CIPSI algorithm (ref 25). [c] CI calculated values after zero-point energy corrections. These are meaningless for the saddle point doubly bridged C_2H_4.

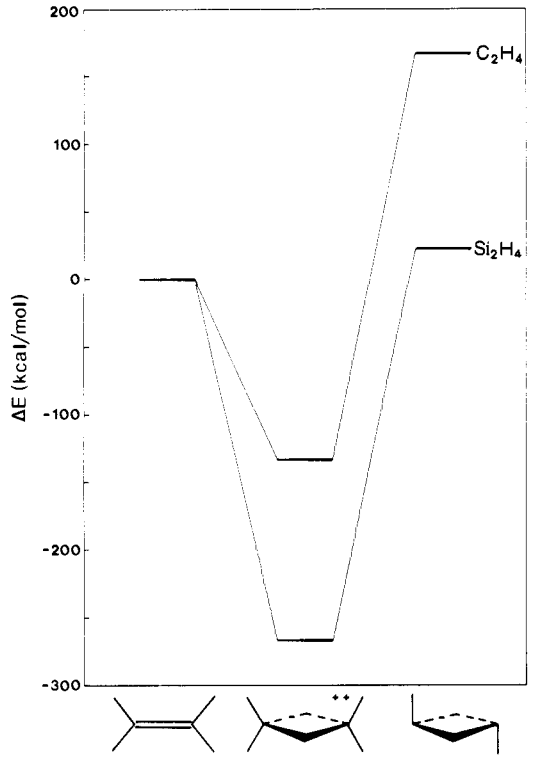

Figure 8. SCF-calculated relative energies for C_2H_4, Si_2H_4, and their diprotonation product. The zero energy is common to the doubly bonded forms.

dibridges such as **18**, with Y = XH_2 (group 13) or XH (group 14), in which one bridge involves a three-center two-electron bond and the other one a three-center four-electron bond.[37]

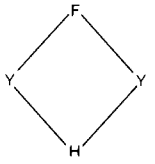

18

The detailed characteristics of a given X–H–X bridge, however, are not data fully transferable from one molecular arrangement to another, since they depend on both the geometry (X···X distance) and the electronic environment at X. This explains why the chemical shift of the bridging hydrogens is quite sensitive to extracyclic substitution, as observed on various derivatives of diborane.[38] It also accounts for the facile modulation and dissymmetrization of the C–H···C part in some μ-hydrido-bridged carbocations.[39]

Table XII. SCF Mulliken Charges and Their Variations under Diprotonation

			double bond	→	$X_2H_6^{2+}$	←	double bridge
net charges	C_2H_4	C	−0.09		+0.09		−0.09
		H_t	+0.05		+0.31		+0.05
		H_b			+0.29		+0.05
	Si_2H_4	Si	+0.23		+0.80		+0.41
		H_t	−0.11		+0.15		−0.18
		H_b			−0.11		−0.23
variations	C_2H_4	C		+0.19	+0.19		
		H_t		+0.26	+0.26		
		H_b			+0.24 (+0.07)[a]		
	Si_2H_4	Si		+0.58	+0.39		
		H_t		+0.27	+0.34		
		H_b			+0.12 (+0.01)[a]		

[a] Values obtained from the (CASSCF + NAMO) results of Table II.

Acknowledgment. The authors thank Dr. I. Garcia-Cuesta for help in the computing part, Drs. J.-P. Daudey, F.-X. Gadéa, and F. Spiegelmann for providing us with computational assistance and routines, and Dr. C. Jouany for helpful discussions.

Appendix

1. SCF Calculations. All the geometries were determined at the SCF level with the PSHONDOG algorithm.[40] This program uses effective core potentials which, for Ga, Sn, and Pb atoms, take into account the mean relativistic effects.[41] Double-ζ + polarization (DZP) basis sets were used. The exponent for the d function on Gallium is taken at 0.16. For the other atoms, the polarization exponents were given in refs 3 and 4. The geometries and harmonic force fields for group 14 X_2H_4 systems were given in ref 3. The geometries for the X_2H_6 molecules and dications are given in Table IX. The corresponding harmonic vibrational frequencies are listed in Table X. All these D_{2h} structures are true minima on the potential surface. For digallane, our geometry is in good agreement with that of ref 6. Moreover, from the analysis of the vibrational frequencies of Table X, the reassignments of infrared frequencies in the spectrum of Ga_2H_6 proposed in that work are confirmed.

2. Expression of the CORP Index in Uncorrelated Simple Schemes. a. Two-Center Two-Electron Heteropolar Bond. Let a and b be the two involved atomic orbitals, **19**, bearing final mean

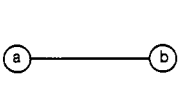

19

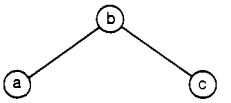

20

electron populations of q on a and $2 - q$ on b. The corresponding molecular orbital is expressed as

$$\varphi = \sqrt{q/2}\,a + \sqrt{1 - q/2}\,b$$

Let us develop the single-determinantal wave function associated with the electron pair

$$\psi = |\varphi\bar{\varphi}|$$

$$\psi = |\sqrt{q/2}\,a + \sqrt{1 - q/2}\,b||\sqrt{q/2}\,a + \sqrt{1 - q/2}\,b|$$

$$\psi = \tfrac{1}{2}\{q|a\bar{a}| + \sqrt{q(2 - q)}(|a\bar{b}| + |b\bar{a}|) + (2 - q)|b\bar{b}|\}$$

(36) Coffy, T. J.; Medford, G.; Plotkin, J.; Long, G. J.; Huffman, J. C.; Shore, S. G. *Organometallics* **1989**, *8*, 2404.
(37) (a) For fluorine bridges in group 14, see: Trinquier, G.; Barthelat, J. C. *J. Am. Chem. Soc.* **1990**, *112*, 9121. (b) For a recent study on Al–F–Al double bridges, see: Rendell, A. P.; Lee, T. J.; Komornicki, A. *Chem. Phys. Lett.* **1991**, *178*, 462.
(38) Leach, J. B.; Ungermann, C. B.; Onak, T. P. *J. Magn. Reson.* **1972**, *6*, 74.
(39) Sorensen, T. S.; Whitworth, S. M. *J. Am. Chem. Soc.* **1990**, *112*, 8135.
(40) Pélissier, M.; Komiha, N.; Daudey, J. P. *J. Compul. Chem.* **1988**, *9*, 298.
(41) Barthelat, J. C.; Pélissier, M.; Durand, Ph. *Phys. Rev. A* **1981**, *21*, 1773.

This provides the elemental probabilities of having 0, 1, or 2 electrons in a given orbital

$$P_a^{(0)} = P_b^{(2)} = (1 - q/2)^2$$

$$P_a^{(1)} = P_b^{(1)} = q(2 - q)/2$$

$$P_a^{(2)} = P_b^{(0)} = (q/2)^2$$

with of course

$$P_{a,b}^{(2)} = 1$$

Reporting these expressions in the relation defining the CORP index

$$\mathrm{CORP} = P_{a,b}^{(2)} - \{P_a^{(1)}P_b^{(1)} + P_a^{(0)}P_b^{(2)} + P_a^{(2)}P_b^{(0)}\}$$

leads to the fourth degree polynomial

$$\mathrm{CORP} = -\tfrac{3}{8}q^4 + \tfrac{3}{2}q^3 - \tfrac{5}{2}q^2 + 2q$$

Such a function is of course symmetrical with respect to $q = 1$, for which the index takes its maximum value of $^5/_8$ (62.5%). Since the tangent in this point is zero, the function keeps close to such a limit as long as the charge contrast remains weak. This was illustrated when the populations of c_1 and c_2 in Table VIII were discussed.

b. Three-Center Two-Electron Symmetrical Bond. Let a, b, and c be the set of atomic orbitals, with a and c playing an equivalent role at terminal positions, **20**. If the final population in a and c is q, that in b is $2 - 2q$. The corresponding occupied molecular orbital is then expressed as

$$\varphi = \sqrt{q/2}(a + c) + \sqrt{1 - q}\,b$$

The associated single determinant now develops as

$$\psi = |\varphi\bar{\varphi}|$$

$$\psi = \tfrac{1}{2}\{q(|a\bar{c}| + |c\bar{a}| + |a\bar{a}| + |c\bar{c}|) + 2(1 - q)|b\bar{b}| + \sqrt{2q(1 - q)}(|a\bar{b}| + |c\bar{b}| + |b\bar{a}| + |b\bar{c}|)\}$$

The ensuing probabilities are

$$P_a^{(0)} = P_{bc}^{(2)} = (1 - q/2)^2$$

$$P_a^{(1)} = q(2 - q)/2$$

$$P_a^{(2)} = (q/2)^2$$

$$P_b^{(0)} = P_{a,c}^{(2)} = q^2$$

$$P_b^{(1)} = 2q(1 - q)$$

$$P_b^{(2)} = (1 - q)^2$$

The definition of CORP thus yields

$$\mathrm{CORP(a–b)} = -\tfrac{3}{2}q^4 + \tfrac{9}{2}q^3 - 5q^2 + 2q$$

$$\mathrm{CORP(a–c)} = -\tfrac{3}{8}q^4 + \tfrac{3}{2}q^3 - \tfrac{1}{2}q^2$$

By using its more general expression,[4] the index can also be extended to the full system, giving a sixth-degree polynomial

$$\mathrm{CORP(a–b–c)} = 1 - \tfrac{1}{4}(1 - q/2)^2(15q^4 - 30q^3 + 29q^2 - 12q + 4)$$

These three indexes are plotted in Figure 6 within all the definition domain of q, which is [0,1] due to the equivalency of orbitals a and c. In this figure, the two vertical lines locate the values of q arising from topological Hückel treatment of the two typical homoatomic cases, namely the allylic cation system ($q = q_a = q_c = {}^1/_2$; $q_b = 1$) and the cyclopropenyl cation (or H_3^+) system ($q = q_a = q_b = q_c = {}^2/_3$). In this homopolar hypothesis, the β'/β ratio would continuously vary from 0 to 1 along this interval. On the extreme boundary $q = 0$, the electron pair is fully located on the b center: there is no bond, all indexes are zero. On the right-hand-side boundary $q = 1$, we turn back to the homopolar two-center bond with the maximal value of $^5/_8$ for CORP(a–c), and of course a zero index for a–b and b–c. Between these two extremes, a–c varies nearly monotonically while a–b exhibits a maximum for a weak population on a and c (0.31e). From pure electronegativity arguments and regardless of the β'/β ratio, the a–b index thus reaches its highest values when the b middle orbital or bridging center is much more electronegative than the terminal counterparts.

The actual CORP indexes calculated from the CASSCF wave functions of the double bridges are plotted in Figure 6, for comparison. They are roughly parallel to the theoretical curves (ignore a–b–c) and are located significantly below them. They run along all the "Hückel zone". The deviation illustrates both the nonabsolute separations of the bridges and significant correlation effects.

3. Diprotonation of C_2H_4 and Si_2H_4. Using different kinds of arguments, let us gauge whether $X_2H_6^{2+}$ is better seen as the diprotonation product of a doubly bonded structure or of a doubly bridged structure.

Geometries. As shown in Figure 7, the criterion of the geometry is not very useful in settling what is closer to what. The top of Figure 7 illustrates how the arrangement of the hydrogens in the planar double bond is close to that of the extracyclic hydrogens in the dication. This similarity is more pronounced in C_2H_4 than in Si_2H_4. The bottom of Figure 7 illustrates how the double bridges are similar in X_2H_4 and $X_2H_6^{2+}$. This time, the proximity is more pronounced in Si_2H_4 than in C_2H_4. On the other hand, the extracyclic (or terminal) hydrogen H_t in neutral doubly bridged Si_2H_4 is almost perpendicular to the ring plane, which is rather far from the extracyclic directions in the dication (see the middle of the figure). This is much more attenuated in C_2H_4 and its dication. Last, note that the XX distance in the dications is lying between that in doubly bonded X_2H_4 and that in doubly bridged X_2H_4. Again, according to this index, $Si_2H_6^{2+}$ is closer to doubly bridged Si_2H_4 than to doubly bonded Si_2H_4. This is further confirmed by the vibrational frequencies.[42] Finally, the doubly bridged dications are like geometrical intermediates between the two isomers of X_2H_4.

Diproton Affinities. The calculated diproton affinities are listed in Table XI. For the same number of electrons, the valence correlation energy is larger in the neutral molecule than in its diprotonated form where the valence electrons are kept in a stronger attractive potential. This decreases the diproton affinities by 4–7 kcal/mol. The zero-point-energy differences further reduce these affinities by ≈10 kcal/mol. The energy contributed by the diprotonation of the doubly bridged form is rather constant (around 300 kcal/mol) for both C_2H_4 and Si_2H_4. The diprotonation of the double bond brings much more energy to Si_2H_4 than to C_2H_4, as a consequence of the energy differences between the two isomers in both series. These relative energies are summarized in Figure 8. Although C_2H_4 is not a real minimum, similar affinities are calculated for the two double bridges C_2H_4 and Si_2H_4, as illustrated by the two parallel lines in the right-hand part of the figure. This suggests that the protonation of the corresponding extracyclic lone pairs is a basically local phenomenon, little affecting the bonding in the bridges. Like the electronic indicators, the energy criterion supports the idea that the diprotonation of the double bond disturbs to a greater extent the bonding in Si_2H_4 than in C_2H_4. The relationships between the double bridges and the dications are visualized in Figure 3. For both C_2H_4 and Si_2H_4, protonation of the extracyclic lone pairs induces a "leftward" shift along our scaling, i.e. toward a higher positive net charge on the bridging hydrogen H_b. This reasonable result leads to the problem of the repartition of the double positive charge.

Where is the Charge? The classical SCF Mulliken net charges are given in Table XII, together with their variations from neutral X_2H_4 to the dication $X_2H_6^{2+}$. For C_2H_4, the diprotonation of the

(42) See Appendix, Section 1 for the geometries and vibrational frequencies of $X_2H_6^{2+}$ and ref 3 for those of X_2H_4.

double bond pushes both atoms toward higher positive charges by fairly comparable amounts, so that all atoms take the charge brought by the $2H^+$. A similar democratic sharing of the charge also occurs from diprotonation of bridged C_2H_4. For Si_2H_4, the net charges are not exactly modified this way. Under diprotonation, the hydrogen atoms of the Si=Si double bond become positively charged and the part of the global charge taken by these hydrogens is about the same as that for C_2H_4. On the other hand, the two protons added to the Si=Si double bond do not contribute to the sharing of the double positive charge, as in the preceding case, since they take a formal negative charge. Therefore, the remainder of positive charge is supported by the silicon atoms. When the Si_2H_4 double bridge is diprotonated, the H_b and H_t hydrogens do not equally share the charge, as was the case for C_2H_4. Now, the bridging hydrogens H_b are little affected and keep a negative charge while the H_t and Si atoms undertake most of the positive charge. The changes brought by the protonation of the lone pairs extracyclic to the double bridge are therefore different in C_2H_4 and Si_2H_4. The structure of the double bridge remains rather unchanged in $Si_2H_6^{2+}$ while it is more perturbed in $C_2H_6^{2+}$. This is also confirmed by the H_b charges calculated from the CASSCF + NAMO procedure. As mentioned in our previous paper,[4] such charges may be very different from the SCF Mulliken ones. However, they are quite in line with the above-discussed trends since the CASSCF charge on H_b is increased more upon protonation for C_2H_4 than it is for Si_2H_4 (see Table XII).

Registry No. B_2H_6, 19287-45-7; Ga_2H_6, 12140-58-8; C_2H_4, 74-85-1; Si_2H_4, 15435-77-5; Ge_2H_4, 82323-93-1; Sn_2H_4, 86041-63-6; Pb_2H_4, 90176-62-8; $C_2H_6^{2+}$, 136061-29-5; $Si_2H_6^{2+}$, 136061-28-4; cyclopropenyl cation, 26810-74-2; allyl cation, 1724-44-3.

Photochemically Induced Dynamic Nuclear Polarization Studies of Oligonucleotide Duplexes

Masato Katahira,[1a,b] Ritsuko Sakaguchi-Katahira,[1a,c] Fumiaki Hayashi,[1a,d] Seiichi Uesugi,[1e] and Yoshimasa Kyogoku*,[1a]

Contribution from the Institute for Protein Research, Osaka University, Suita, Osaka 565, Japan, and Faculty of Pharmaceutical Sciences, Osaka University, Suita, Osaka 565, Japan.
Received December 10, 1990

Abstract: The application of the photochemically induced dynamic nuclear polarization (photo-CIDNP) technique to structural studies of nucleic acids has been attempted. The CIDNP signals of double-stranded nucleic acids were observed for the first time. The CIDNP signals were observed clearly for A and B form oligonucleotides examined, $r(CGCGCG)_2$ and $d(CGCGCG)_2$ in 0.15 M NaCl, respectively, while those for Z form oligonucleotides examined, $r(CGCGCG)_2$ and $d(CGCGCG)_2$ in saturated $NaClO_4$, were very weak. The central two guanosine residues of $d(GGGGCCCC)_2$ give an intense CIDNP signal, which disappears when the drug, chromomycin, binds to the minor groove of this oligonucleotide. The most likely explanation for this result is that chromomycin bound to the minor groove interferes with the access of a flavin molecule to the base and prevents the photoreaction indispensable for the appearance of the CIDNP signal. The correlation between the unusual cutting of some oligonucleotides by the drug, bleomycin, and their CIDNP signals was also found. The results presented here indicate the possible application of the photo-CIDNP technique to structural studies of nucleic acids.

The photo-CIDNP technique is a very unique ^1H NMR spectroscopic technique and has been applied successfully to proteins to study their surface structure and their interactions with ligands (see Kaptein[2] for a review). On the other hand, its application to nucleic acids has been limited to mononucleotides,[3-5] dinucleotides[4,6] and the single-stranded region of tRNA.[7] It has been believed that this technique is only useful for detecting single-stranded nucleic acids, i.e., not for structural studies of double-stranded nucleic acids because CIDNP signals have not been observed for double-stranded nucleic acids such as $d(CGCG)_2$[8] and $r(AGCU)_2$.[5] Here, however, we observed the CIDNP signals of double-stranded nucleic acids for the first time, and the relationship between the appearance of the CIDNP signals and the structures of nucleic acids has been studied.

Previous studies showed that the base protons of purine bases, guanine and adenine, give rise to the CIDNP signals.[3,5] The presence of the guanine, however, suppresses the CIDNP signal of the adenine.[5] Therefore, we concentrated on the CIDNP signal of the base proton of the guanine, the H8 proton. First, in order to investigate the structure-dependency of the CIDNP signals of double-stranded nucleic acids, the CIDNP signals of the following oligonucleotides were examined: $r(CGCGCG)_2$ in 0.15 M NaCl (A form), $d(CGCGCG)_2$ in 0.15 M NaCl (**B** form), and $r(CGCGCG)_2$ and $d(CGCGCG)_2$ in saturated $NaClO_4$ (Z form). Secondly, the CIDNP signals of $d(GGGGCCCC)_2$ and the chromomycin-$d(GGGGCCCC)_2$ complex, where an antitumor drug, chromomycin, is bound to the minor groove of this oligo-

* Correspondence should be addressed to: Professor Yoshimasa Kyogoku, Institute for Protein Research, Osaka University, 3-2, Yamadaoka, Suita, Osaka 565, Japan. Telephone: 81(Japan)-68779725; Fax: 81(Japan)-68762533.

(1) (a) Institute for Protein Research, Osaka University. (b) Present address: Department of Chemistry, University of Utrecht, Padualaan 8, 3584 CH Utrecht, The Netherlands. (c) Present address: International Research Laboratories, CIBA-GEIGY JAPAN, Miyuki-cho, Takarazuka, Hyogo 665, Japan. (d) Present address: Research Laboratory, Shionogi Pharmaceutical Company, Sagisu, Fukushima-ku, Osaka 553, Japan. (e) Faculty of Pharmaceutical Sciences, Osaka University.

(2) Kaptein, R. *Biological Magnetic Resonance*; Plenum: New York, 1982; pp 145-191.
(3) Kaptein, R.; Nicolay, K.; Dijkstra, K. *J. Chem. Soc. Chem. Commun.* **1979**, 1092-1094.
(4) Scheek, R. M.; Stob, S.; Schleich, T.; Alma, N. C. M.; Hilbers, C. W.; Kaptein, R. *J. Am. Chem. Soc.* **1981**, *103*, 5930-5932.
(5) McCord, E. F.; Morden, K. M.; Pardi, A.; Tinoco, I, Jr.; Boxer, S. G. *Biochemistry* **1984**, *23*, 1926-1934.
(6) Kaptein, R.; Stob, S.; Scheek, R. M.; Dijkstra, K.; Schleich, T. W. *Bull. Magn. Reson.* **1981**, *3*, 28-30.
(7) McCord, E. F.; Morden, K. M.; Tinoco, I, Jr.; Boxer, S. G. *Biochemistry* **1984**, *23*, 1935-1939.
(8) Garssen, G. J.; Kaptein, R.; Schoenmakers, J. G. G.; Hilbers, C. W. *Proc. Natl. Acad. Sci. U.S.A.* **1978**, *75*, 5281-5285.

0002-7863/91/1513-8647$02.50/0